Physical Modeling and Simulation of Polymeric Structures with Metallic Material Printed by Electrically Assisted Vat Photopolymerization for Property Enhancements

by

Lakshya Tiwari

A Thesis Presented in Partial Fulfillment
of the Requirements for the Degree
Master of Science

Approved April 2023 by the
Graduate Supervisory Committee:

Xiangjia Li, Chair
Sui Yang
Linqin Mu
Beomjin Kwon

ARIZONA STATE UNIVERSITY

May 2023

ABSTRACT

Applications like integrated circuits, microelectromechanical devices, antennas, sensors, actuators, and metamaterials benefit from heterogeneous material systems made of metallic structures and polymer matrixes. Due to their distinctive shells made of metal and polymer, scaly-foot snails, which are found in the deep ocean, exhibit high strength and temperature resistance. Recent metal deposition fabrication techniques have been used to create a variety of multi-material structures. However, using these complex hybrid processes, it is difficult to build complex 3D structures of heterogeneous material with improved properties, high resolution, and time efficiency. The use of electrical field-assisted heterogeneous material printing (EFA-HMP) technology has shown potential in fabricating metal-composite materials with improved mechanical properties and controlled microstructures. The technology is an advanced form of 3D printing that allows for printing multiple materials with different properties in a single print. This allows for the creation of complex and functional structures that are not possible with traditional 3D printing methods. The development of a photocurable printing solution was carried out that can serve as an electrolyte for charge transfer and further research into the printing solution's curing properties was conducted. A fundamental understanding of the formation mechanism of metallic structures on the polymer matrix was investigated through physics-based multiscale modeling and simulations. The relationship between the metallic structure's morphology, the printing solution's properties, and the printing process parameters was discovered.

The thesis aims to investigate the microstructures and electrical properties of metal-composite materials fabricated using EFA-HMP technology and to evaluate the correlation between them. Several samples of metal-composite materials with different microstructures will be fabricated using EFA-HMP technology to accomplish this. The results of this study will provide a better understanding of the relationship between the microstructures and properties of metal-composite materials fabricated using EFA-HMP technology and contribute to the development of new and improved materials in various fields of application. Furthermore, this research will also shed light on the advantages and limitations of EFA-HMP technology in fabricating metal-composite materials and study the correlation between the microstructures and mechanical properties.

ACKNOWLEDGMENTS

I would like to begin by expressing my sincere gratitude to Professor Xiangjia Li, my advisor, for offering me the opportunity to work as a Research Aide in the Lab of Manufacturing Innovations, and for her constant support, guidance, and encouragement throughout my thesis research. I am truly grateful for the countless hours she spent with me over the past two academic semesters, providing me with valuable advice on how to handle various situations and leading me on my quest for knowledge with infinite patience and mentorship. I would also like to extend my heartfelt thanks to the members of my committee, Professors Sui Yang, Linqin Mu, and Beomjin Kwon.

I would like to acknowledge and appreciate the invaluable assistance, original suggestions, and unwavering support that my lab mate, Tengteng Tang, provided me with throughout my research. Without their help, I could not have achieved my research goals. I would also like to thank the Eyring Materials Center, located in the PSB - Bateman Physical Sciences Center B Wing, B154A, for allowing me to use their SEM/FIB Focused Ion Beam - Auriga (Zeiss) for my research.

Furthermore, I would like to express my deepest gratitude to my family and friends for their love, support, and encouragement throughout my graduate studies. Their unwavering support and belief in me have been a constant source of motivation and inspiration. Lastly, I would like to thank all my lab mates, colleagues, mentors, and advisors for their support and assistance during my degree. I am truly grateful for their unwavering commitment to my success.

TABLE OF CONTENTS

Page

LIST OF FIGURES

Figure Page

Figure Page

Figure Page

Figure Page

CHAPTER 1 INTRODUCTION

Over millions of years of evolution, natural organisms have developed intricate hierarchical structures with highly integrated materials, structures, and functions that serve as a model for creating high-performance functional devices. Biomimicry makes possible a previously unexplored path for designing and producing useful devices with top-notch mechanical, electromagnetic, and hydrodynamic properties. Meanwhile, AM overcomes the limitations of conventional manufacturing techniques and enables bionic manufacturing. [1-2] For instance, the metallic exterior of a scaly-foot snail (Figure 1a) that dwells in a hydrothermal vent in the deep sea has caught the interest of scientists. Greigite, Fe_3S_4, a layer of iron sulfide with a thickness of about 30 μm, makes up most of the outer layer of its shell. [3] This substance, which gives its shell its extreme hardness and excellent high-temperature resistance, does not exist in the skeleton of any other species. Because of their potential applications in defense, energy dispersion, sensing, and microelectronic-mechanical systems, heterogeneous material systems based on metallic structures and polymer matrixes have emerged as promising research areas (Figure 1b). [4] However, using modern manufacturing technologies, more research needs to be done on how to bio-imitate such a scaly-foot snail to enhance its properties.

Metal-polymer composites are a type of material composed of metal particles or fibers embedded in a polymer matrix. These composites have been gaining popularity in recent years due to their unique properties, combining the

advantages of metal and polymer materials. One of the main advantages of metal-polymer composites is that they can be tailored to specific applications by controlling the size, shape, and distribution of the metal particles or fibers within the polymer matrix. For example, by using smaller metal particles or fibers, it is possible to increase the strength and stiffness of the composite, while larger particles or fibers can be used to improve thermal conductivity and electrical conductivity.[5] The main challenge is how to manufacture metallic materials using a polymer matrix all at once as opposed to the conventional approach of using multiple processes, particularly when using electrodepositing to create metallic structures from conductive polymers. Several hybrid metallization technologies have recently surfaced to address the issues by integrating with AM processes. For instance, Hudkins et al. showed that it was possible to print electrodes out of conductive PLA/carbon polymer composites, and then nickel was electroplated onto the 3D-printed objects.[6] Rosa-Ortis et al. created conductive 3D parts using the same commercially available composite filament and coated additional metal layers using the hydrogen-assisted electroplating (HAE) technique.[7] To print 3D objects and then selectively electroplate the conductive domain to create 3D circuit boards, Lazarus et al. used dual extruder heads filled with conductive PLA/copper and non-conductive ABS filament (Figure 1d).[8] Similar research was done by printing 3D parts from conductive and nonconductive filaments, and then selectively electroplating 3D metallic structures on the conductive surfaces.[9] Additionally, using mask image projection-based stereolithography, Ryan et al. printed 3D structures with a programmable mosaic of surface charge region (MIP-

SL). It enables the selective deposition of single metals for the fabrication of electronic devices from multiple materials.[10] The methods mentioned above involve several difficult and drawn-out steps. Additionally, the printed objects are not firmly attached to the plated layer, which exacerbates issues with cracking, non-uniform microstructures, and hardenability. To increase the efficiency of fabrication, researchers worked hard to create new processes that can print metal/polymer structures in a single step. For instance, Zhao et al. created a polymer-assisted photochemical deposition-based room-temperature metal/polymer printing process. This method allows for the fabrication of silver, gold, and platinum on a variety of substrates (Figure 1c).[11] Like this, metallic silver was printed using visible light projection lithography at room temperature on polymer substrates.[12] However, the current photochemical deposition-based 3D printing technology is limited to a few types of metals and metal/polymer hybrid structures.

Here an innovative method called electrical field-assisted heterogeneous material printing (EFA-HMP) is used, which can control the metallic structures deposition on the polymer matrix composite for improved functional characteristics, to address the current difficulties in the 3D printing of heterogeneous materials systems made of metal and polymer at room temperature. Using currently available methods makes it challenging to fabricate metallic structures in a single step at room temperature. Using a polymer matrix-based composite, which was developed in this study, it was possible to maintain the transport of metallic ions and encourage metal deposition on a photocured

polymer matrix. Poly (3,4-ethylene dioxythiophene)-poly(styrene sulfonate) (PEDOT: PSS) was combined with poly(ethylene glycol) diacrylate (Mn 700) (PEGDA) and poly(ethylene glycol) diacrylate (Mn 250) (PEGDA), which is frequently used in the fabrication of flexible sensors due to its biocompatibility [13, 14] to increase the electrical conductivity of photocurable resin.

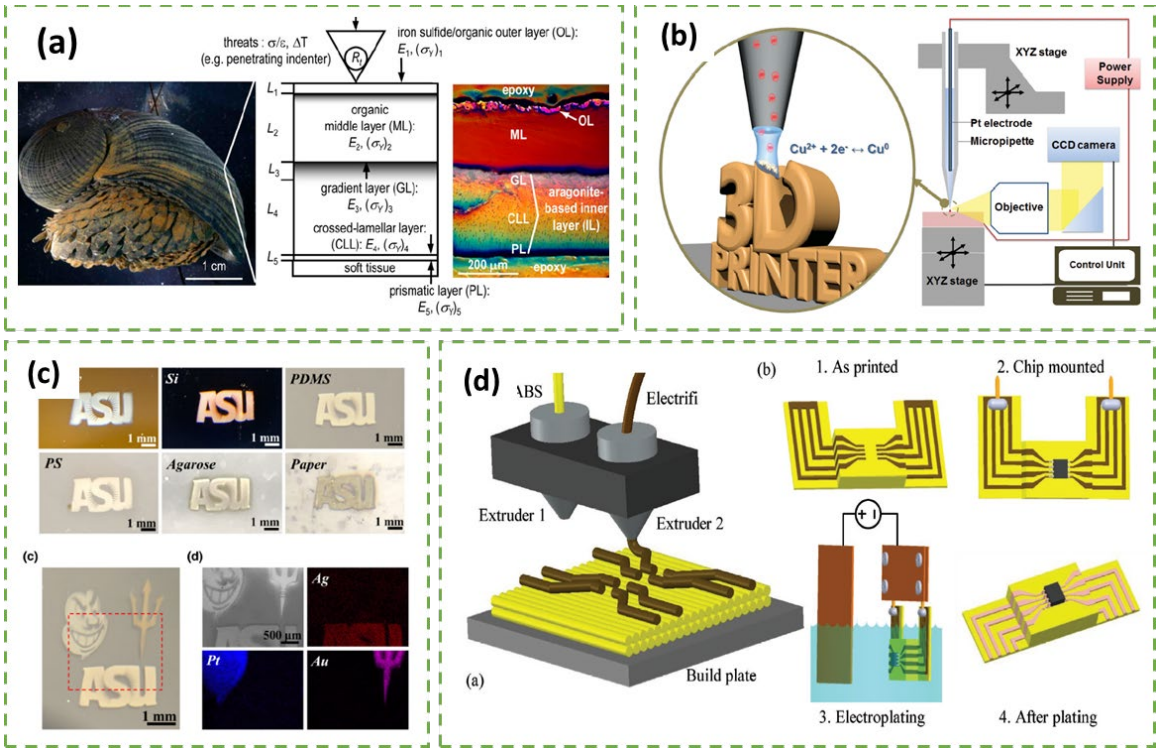

Figure 1: a) Macroscopic and microscopic multilayered structure of the shell of the entire snail.[3] b) Schematic illustration of the electrodeposition-based 3D printing apparatus.[4] c) Metal patterns printed on various substrates with SEM.[11] d) Dual extrusion fused filament fabrication and electroplating process.[8]

In addition, the inorganic substances were included to supply adequate metal ions for the deposition. The parameters of the recently created printing solution, such as exposure time, cure depth, viscosity, and resistivity, are then further investigated. For the metal deposition, the electrical field generation module was

developed and integrated with MIPSL. Metallic structures can develop during the printing process on the curing polymer matrix by regulating the electrical field (Figure 2). Metal ion concentration, electrical field voltage, and deposition time are factors that affect how quickly metallic structures are formed.[15]

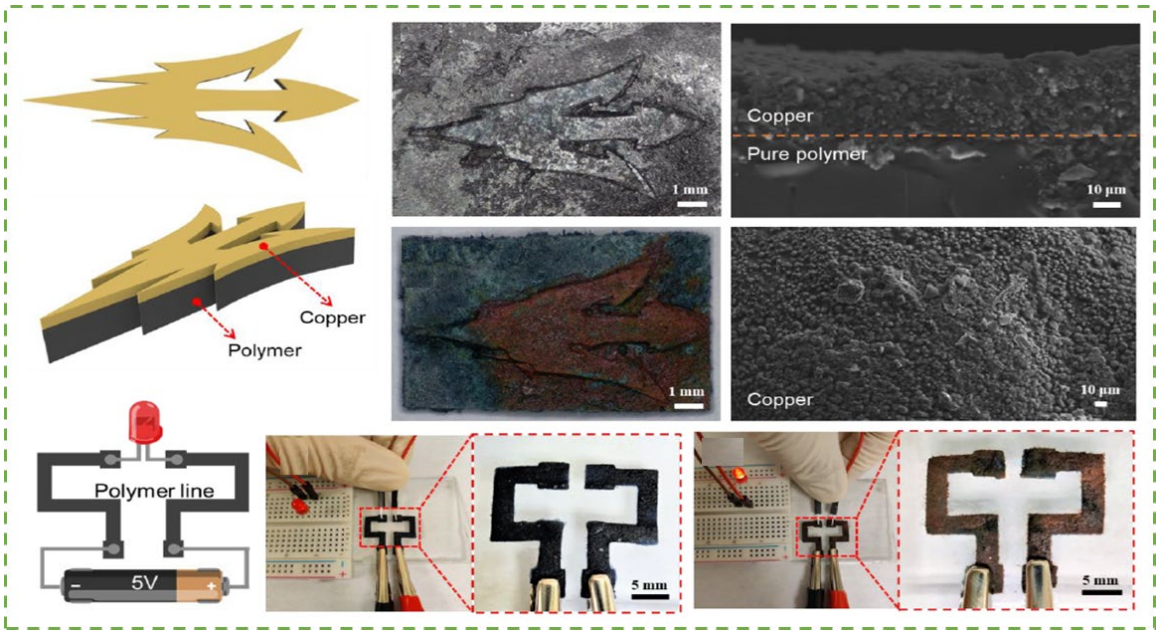

Figure 2: Electrical field-assisted heterogeneous material printing of polymeric material with metallic structures for different applications.[15]

The process parameters were optimized based on physics-based modeling, simulation, and testing to produce accurate printing of polymer/metal material systems with desired geometric shapes. It discovered the relationship between the geometric morphology, the characteristics of the material, and the printing process settings.

1.1 Background

Polymer Metal Composites (PMCs) are a class of hybrid materials that combine the properties of polymers and metals to produce materials with unique

mechanical, electrical, and thermal properties. Even while 3D printing has made it feasible to quickly prototype a variety of 3D buildings, only a relatively small number of designs have taken advantage of this technology to produce structures that are challenging or impossible to manufacture in any other method.[16] The adoption of 3D printing technologies can undoubtedly help electrochemistry since they make it easier to build complicated measurement systems that are unique to the field at a lower cost and with greater variety. 3D printing can be used to create conductive electrodes with unique shapes or compositions for use in redox and catalytic processes. It can also be used to construct liquid handling systems, including voltammetric cells or micro-microfluidic systems, which can be combined with electrodes.[17] Another major application for polymer/metal structures is in the aerospace industry. These structures are often used in the production of aircraft parts such as fuselage panels and wing spars. The high strength-to-weight ratio of polymer/metal structures makes them well-suited for use in aircraft parts, as they can provide strength and rigidity without adding significant weight.[18] Micro-dispensing direct-print additive manufacturing (DPAM) and FDM methods were used to create flexible antennas. The method helps produce 3D conformal designs, enables the rapid printing of conductors with high dimensional control, and allows for the printing of conductors on relatively smooth surfaces of FDM-printed substrates (Figure 3a).[19] High-resolution Stereolithography 3D printing is combined with a different novel surface modification technique to enable arbitrary 3D antenna designs that have never been seen before,

such as a Voronoi tessellation for low volume, lightweight, and aerodynamic properties, and 3D fractal geometries with comparable physical benefits (Figure 3b).[20]

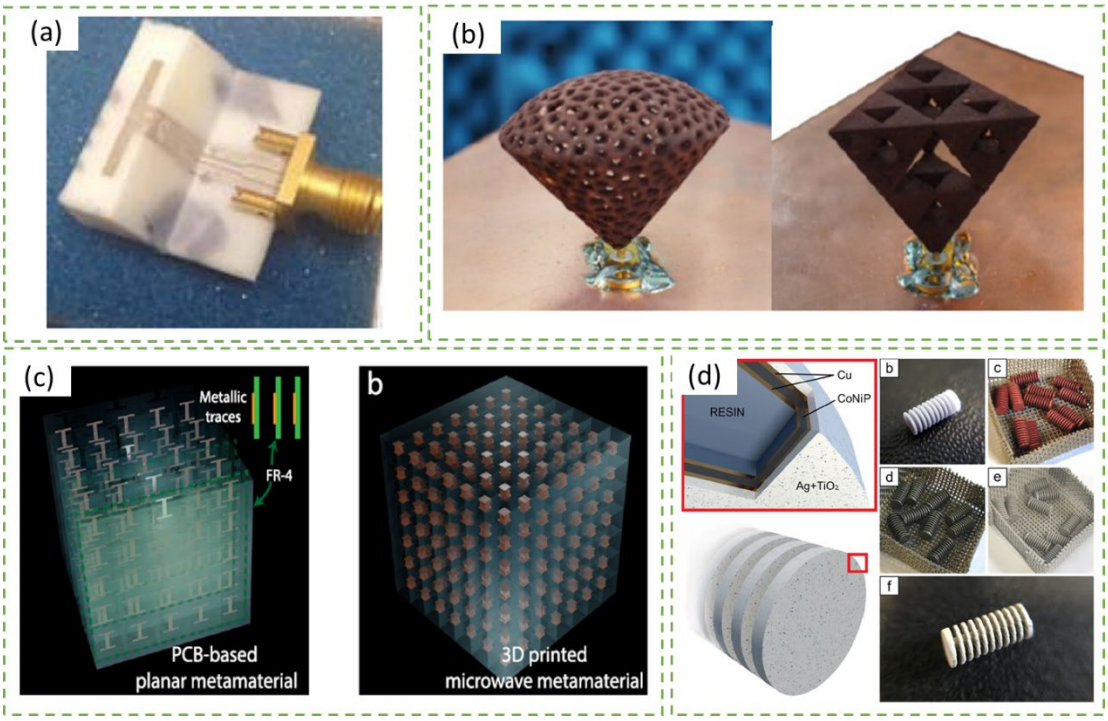

Figure 3: a) Manufactured 6.0 GHz antenna superstrate removed to show the conformal circuity.[19] b) Voronoi inverted feed discone and Fractal Sierpinski triangle antenna.[20] c) Schematics of a conventional PCB-based metamaterial and a 3D-printed metamaterial.[22] d) Internal structure of the photoactive/antimicrobial devices.[21]

Stereolithography 3D printing, wet metallization, and other techniques are used to create micro robotic prototypes for cleaning water. To add the necessary functions, various metallic layers are plated via electroless and electrolytic deposition on 3D-printed parts. For the first time on the same device, bacteria-killing, and pollutants photodegradation are coupled by coating it with a composite nanocoating made of titania nanoparticles in a silver matrix, which takes advantage

of the adaptability and plasticity of electrolytic co-deposition. By applying rotating magnetic fields, the microstructure of the resulting microrobots (Figure 3d) is fully described, and they are successfully operated.[21] By 3D printing a highly conductive polymer composite filament using fused deposition modeling, three-dimensional microwave metamaterials can be created. For applications involving microwave metamaterials, it is demonstrated that the conductivity of such a filament is almost identical to that of a perfect conductor. Designing, making, and testing a 3D-printed unit cell with a broadband permittivity as high as 14.4 shows the increased degrees of freedom made possible by 3D metamaterial designs (Figure 3c). With a mean squared error of less than 0.1, the simulated and measured S-parameters accord well.[22]

1.2 Metal Polymer fabrication using traditional techniques.

Metal fibers or particles are incorporated into a polymer matrix during the creation of metal-polymer composites. The composite's intended qualities will determine the metal and polymer to use. Aluminum, copper, and nickel are the most often used metals, whereas epoxy, polyethylene, and polypropylene are the most frequently used polymers. Metal-polymer production can be done using welding, a conventional manufacturing method. In this procedure, components made of metal and polymer are fused by being heated to a high temperature and put under pressure. DPK 30/50+ZE dual-phase steel cover sheets that were electrolytically galvanized and a polypropylene-polyethylene foil core material were used to create a three-layered metal-polymer-metal sample. Using Nd: YAG

ROFIN StarWeld Manual Performance laser, the samples were welded on both sides (Figure 4a).[23] Whereas in friction stir welding, a cylindrical tool with a profiled pin is rotated and inserted into the plate material's adjoining edges. To prevent the joint faces from being driven apart, the pieces must be tightly fastened. The wear-resistant welding tool can move along the weld line because frictional heat between the workpieces and the tool causes the latter to soften without melting. The material that has been plastically softened is transferred to the tool pin's trailing edge and forged by the close contact of the tool shoulder and pin profile. It leaves a strong phase link between the two components after cooling (Figure 4b).[24] The method used to prepare the surface of the metal composite layers is like the method used to adhere materials together. To achieve the strongest adhesive bonding possible, surface preparation should be helpful. To achieve this requirement, it is required to clean impurities from the attached surfaces' surfaces to get the right surface roughness for the combined materials and the right surface energy for the treated surface. Applying an adhesion promoter, mechanical treatment (such as grinding and sandblasting), and chemical or electrochemical treatment are the three fundamental surface-treatment techniques (e.g., etching with hydrofluoric acid and dry surface treatments). Following the preparation of the sheet's surface and the fiber for the reinforced plastics, they are stacked alternately, with the metal layers acting as the composite's outside components. Metallic sheets may be mixed with alternating layers of polymer films and fibers to create FML as an alternative to making it from prepregs and metallic sheets. The

ingredients are then properly layered and bonded using pressure and heat (Figure 4c).[25]

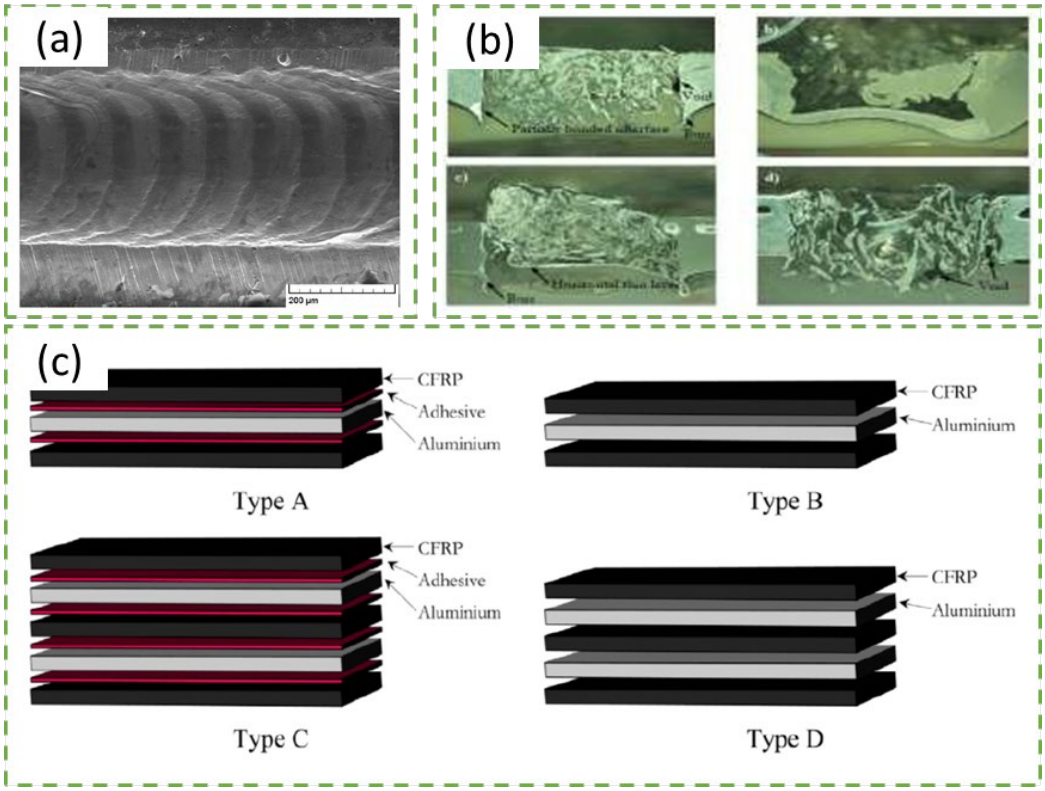

Figure 4: a) Top view of the welded joint.[23] b) The micrographs of aluminum-thermoplastic joint cross.[24] c) Stacking sequence of FMLs.[25]

1.3 Metal Polymer fabrication using hybrid techniques.

Hybrid manufacturing is an advanced manufacturing method that combines different techniques to achieve the best properties of each. It can also be used in metal-polymer fabrication. By combining traditional manufacturing techniques such as casting, welding, and machining with advanced techniques such as 3D printing, hybrid manufacturing can be used to create complex and highly customized metal-polymer materials. One example of hybrid manufacturing in metal-polymer fabrication is the use of 3D printing to create complex and highly

customized polymer molds for casting. The study of hybrid metal/polymer composite filaments has made it possible to print metal items using the conventional Fused Filament Fabrication (FFF) technique. Through cycles of debinding and sintering, the resulting hybrid metal/polymer part can subsequently be converted into a dense metal part. The 17-4 PH samples were printed and sintered in-house utilizing a Metal X printer under Markforged's recommended printing parameters. By using specialized software called Eiger, the part size and all other ADAM process parameters, including the support structure, are automatically designed (Figure 5a).[26] Another study investigated the creation of metal/polymer composites utilizing polyethylene as the matrix and different metal powder compositions. One of the most common and traditional additive manufacturing processes, fused deposition modeling (FDM), produces three-dimensional (3D) specimens from computer-aided design data with complex geometry at a cheaper cost than alternative processes. In this study, a compounding production line was used to create composite filaments for the FDM process that contained 25, 50, and 75% copper powder. Flexural, electrical conductivity, and bulk density tests were conducted once printing-related (Figure 5b) difficulties were resolved. Scanning electron microscopy was used to study the specimens' micrographs to determine how the copper particles were distributed.[27]

The initial compositing process and the surface electroding process are two separate preparation procedures that are included in the most cutting-edge IPMC manufacturing approach currently available. The morphologies of the precipitated platinum varied greatly because of the various preparation methods. In the context

of chemical reduction procedures comparable to the processes, the initial compositing step needs a suitable platinum salt. The idea behind the composition method is to use chemical reduction to metalize the material's inner surface, which is typically covered in Pt nanoparticles in the shape of membranes. To enable platinum-containing cations to permeate through via the ion exchange process, the ion exchange polymer is submerged in a salt solution. Then, a suitable reducing agent is added to molecularly plate the materials and platinize them.[28]

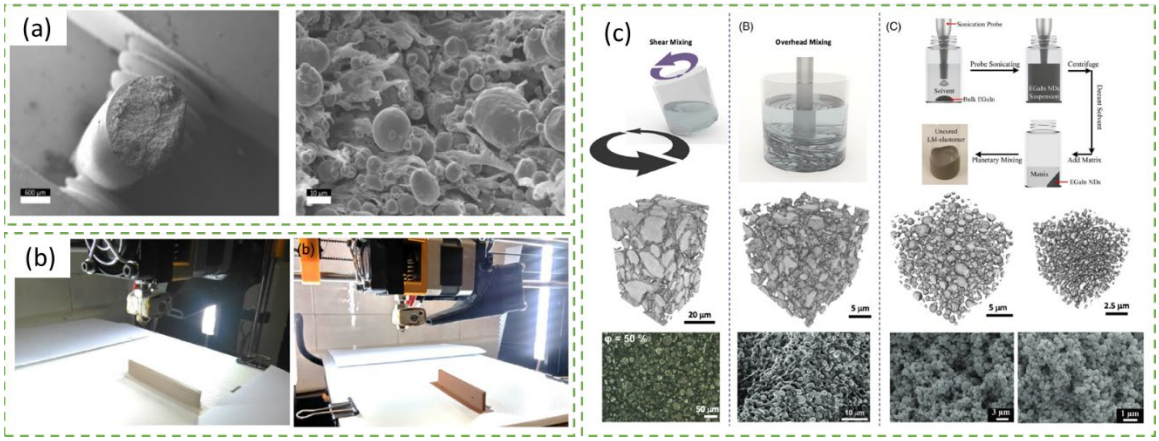

Figure 5: a) Cross-section SEM analysis of the Ultrafuse 316L filament.[26] b) Printed PE-based specimens: pure PE and Cu–PE composite.[27] c) Controlled microstructures in liquid metal elastomer composites through processing parameters.[29]

A new family of functional materials called liquid metal-polymer composites has the potential to revolutionize wearable electronics, soft robotics, and human-computer interfaces. Several processing techniques can be used to embed room-temperature liquid metal inclusions in insulating polymers like elastomers, incorporating the functional qualities of metals while keeping the matrix flexible and soft. The multifunctional material system that these solid-liquid composites offer is intriguing but difficult. A unique overview of the synthesis processes, structural and

functional characteristics, and applications of gallium-based liquid metal polymer composites are provided in this paper. There is a discussion of common techniques for regulating the size of liquid metal inclusions and their interaction with polymers. Also, a summary is provided of how liquid metal microstructures affect the general characteristics of the composites. Synthesis methods include Planetary shear mixing, Overhead mixing as well as Sonication (Figure 5c).[29]

1.4 Challenges

The difficulty of putting metal and polymer materials together is one of the key obstacles in metal-polymer fabrication, which can create various difficulties when employing conventional manufacturing procedures. Strong bonds between these materials may be challenging to achieve due to their different physical characteristics. These materials might not be successfully joined using conventional joining methods like brazing and welding. Due to the various thermal expansion coefficients of metal and polymer materials, it might be challenging to keep the material's integrity when exposed to temperature changes. Warping, cracking, and other types of material failure can result from this. Creating a uniformly smooth surface finish in metal-polymer manufacturing is another problem. The difference in properties of metal and polymer can make it difficult to achieve a consistent surface finish. This can also affect the aesthetics of the final product.[30] The density of the metal-polymer distribution in the form, the rheology of the metal-polymer in the mold channels, the thermal degradation of the metal-polymer during abrasive processing, and the lack of technological support for

pouring metal polymer into a mold are some additional problems that arise during the manufacture of metal-polymer composite structures. Throughout the fabrication process, the metal and polymer employed should be able to withstand both chemical and physical reactions. When certain metals and polymers are combined, chemical reactions can occur that can cause the material's characteristics to deteriorate and its structural integrity to be lost. Complex geometries and shapes could be challenging to fabricate using conventional production methods. This can be particularly problematic when attempting to reproduce complex patterns or organic shapes. The combination of metal and polymer can be more expensive than using a single material, especially if it requires special machinery and processing.[31]

Complex geometries and shapes could be challenging to fabricate using conventional production methods. This can be particularly problematic when attempting to reproduce complex patterns or organic shapes. If specialized equipment and processing are needed, combining metal and polymer may be more expensive than utilizing just one material. The right metal, polymer, and manufacturing process must be carefully chosen to overcome these obstacles. Additionally, the utilization of cutting-edge methods like computer-aided design and manufacturing, simulation, and testing can aid in the optimization of the fabrication process and guarantee the quality and integrity of the finished product. [32] For inkjet and microfluidic applications, monolithic polymer-metal microstructures can be created employing two different types of photoresists and electroforming processes. Just topside exposure is applied to various resists in

conventional integrated technology; however, it will have a severe shrinkage problem. As a result, the resist coating that comes next will be uneven and crowded where exposed and hidden parts meet. Moreover, the rough surface caused by shrinkage to the electroformed nozzle plate is duplicated.[33]

1.5 Motivation & Objective

The goal of metal-polymer manufacturing is to produce materials with special qualities that are impossible to attain with either material alone. Scientists and engineers can produce materials with better strength, flexibility, thermal stability, and other qualities that are perfect for a variety of applications by fusing the advantages of the two materials. Improving the finished material's mechanical characteristics is one of the key goals of metal-polymer manufacturing. Materials that are stronger and longer lasting than those made from a single material can be produced when metal and polymer are combined. A further goal of metal-polymer fabrication is to raise the final product's thermal stability. The material's polymer and metal components both can give flexibility and thermal stability. By combining the chemical resistance of the polymer with the metal's corrosion resistance, metal-polymer materials can be created with improved corrosion resistance. Functional materials with distinctive qualities including electrical conductivity, thermal conductivity, and magnetic characteristics can be made by mixing metal and polymer components. Metal-polymer compounds can help to lighten the end product's weight while strengthening it by including polymer components. By adjusting the composition, structure, and processing conditions, metal-polymer

composites' characteristics can be improved. For instance, the mechanical, thermal, and electrical properties of metal polymers can be enhanced by the inclusion of nanomaterials like graphene, carbon nanotubes, and nanoparticles.

The creation of materials with increased biocompatibility for use in biomedical applications is another goal of metal-polymer composite manufacturing. Because of their high strength and resistance to corrosion, metals like titanium and stainless steel are frequently utilized in biomedical implants. These metals, meanwhile, have the potential to have negative effects on the body and result in implant failure. In metal-polymer composites, the incorporation of polymer components might enhance biocompatibility by minimizing unfavorable reactions brought on by metals. Due to the various characteristics and shapes of the materials employed, metal-polymer manufacturing offers a wide range of customizing options. When opposed to employing a single material, metal-polymer production can be more affordable, particularly if it calls for specialized equipment and processing. Creating materials with enhanced qualities that may be used in a variety of applications, including aerospace, automotive, medical, construction, and many others, is the primary driving force behind metal-polymer fabrication. Metal-polymer manufacturing aims to create materials with improved mechanical properties, increased thermal stability, increased corrosion resistance, created functional materials, increased strength, decreased weight, and cost-effectiveness.

This study's goal is to examine the relationships between the electrical characteristics and microstructures of metal-composite materials made with EFA-

HMP technology. To do this, a variety of samples of metal-composite materials with various microstructures are created utilizing EFA-HMP technology. Without the need for any further steps, the resin enables us to print the structure layer by layer and simultaneously coat it with copper metal. The findings of this study will help develop new and better materials for use in a variety of domains of application and provide a better knowledge of the relationship between the microstructures and properties of metal-composite materials made utilizing EFA-HMP technology.

CHAPTER 2 LITERATURE REVIEW

2.1 Stereolithography

Stereolithography (SLA), the first type of additive manufacturing, creates 3D things by selectively solidifying liquid resin using a photopolymerization reaction. Stereolithography has received a lot of interest because of its capacity to produce items with great accuracy using a wide range of materials. Over the past 40 years, SLA has undergone four main technological generations since its creation in the 1980s. As a result, a wide variety of stereolithography methods (Figure 6) have been developed, each with significantly better resolution, throughput, and material options for building intricate 3D devices.[34] A vat of liquid photopolymer resin, which is UV-sensitive, is the first step in the SLA process. A single layer of the finished part's surface is targeted by a laser beam that selectively cures (hardens) the resin in that pattern. The following layer is then cured on top of the preceding one after the platform on which the part is being constructed is lowered by a modest amount, typically between 0.05 and 0.15mm. Until the portion is finished, this process is repeated.[35] One of the key advantages of SLA is its ability to produce parts with very high resolution and fine details, which makes it suitable for creating intricate models and prototypes. The surface finish of SLA parts is also very smooth, which is an added advantage for parts that require a high-quality surface finish. However, there are some drawbacks associated with SLA as well. The size of the build volume is one of the key restrictions. The size of the items that can be printed is constrained by SLA printers since they typically have a lower

build volume than other 3D printing methods. SLA often takes longer than other 3D printing techniques since each layer needs to be separately cured, such as FDM (Fused Deposition Modeling) and SLS (Selective Laser Sintering). Additionally, SLA parts can be brittle and can be damaged if subjected to stress or impact. It also requires special handling and post-processing, such as cleaning and curing the parts before use.[36]

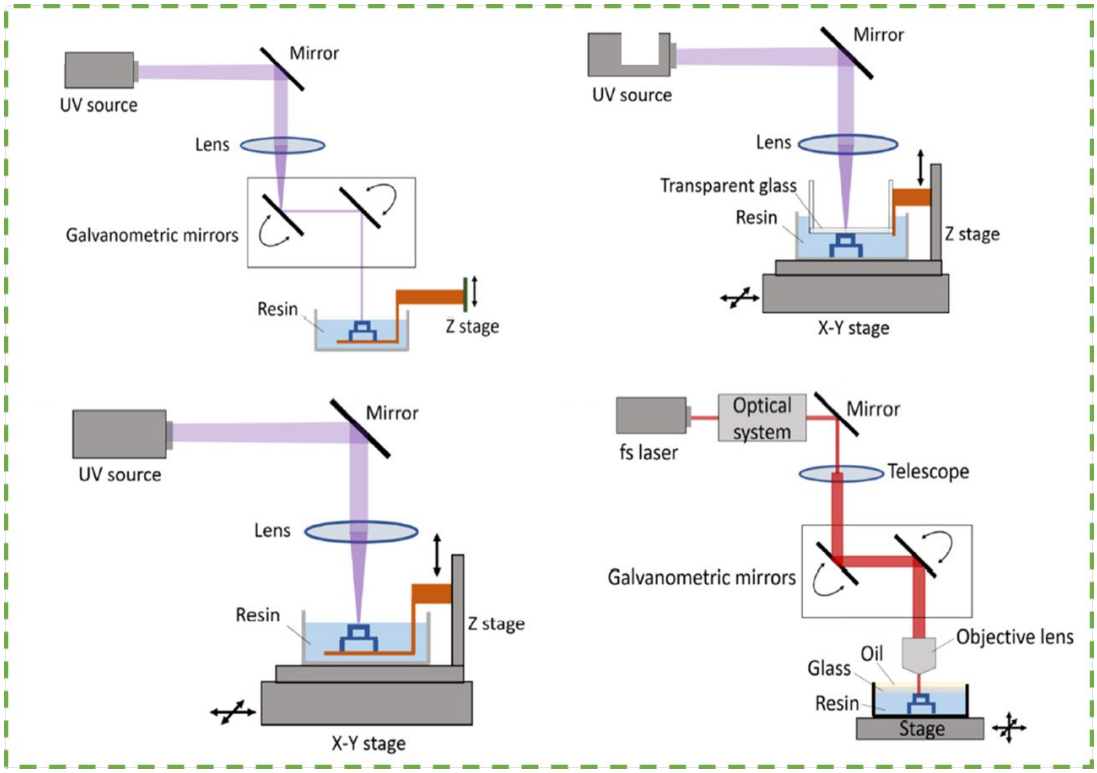

Figure 6: Scanning stereolithography processes.[34]

The approximation of the part before production and the building and finishing of the part are two categories of mistakes that have an impact on the accuracy of SL parts. In the part-building process, there are primarily two types of defects: curing errors and control errors. Errors resulting from over-curing and scanning line form are referred to as curing errors. Control errors are those brought

on by control over the layer thickness and scan position. There are errors caused by the finishing process in addition to errors created during the part's construction. Stair step, tessellation, and slicing mistakes are examples of approximation errors in part models.[37]

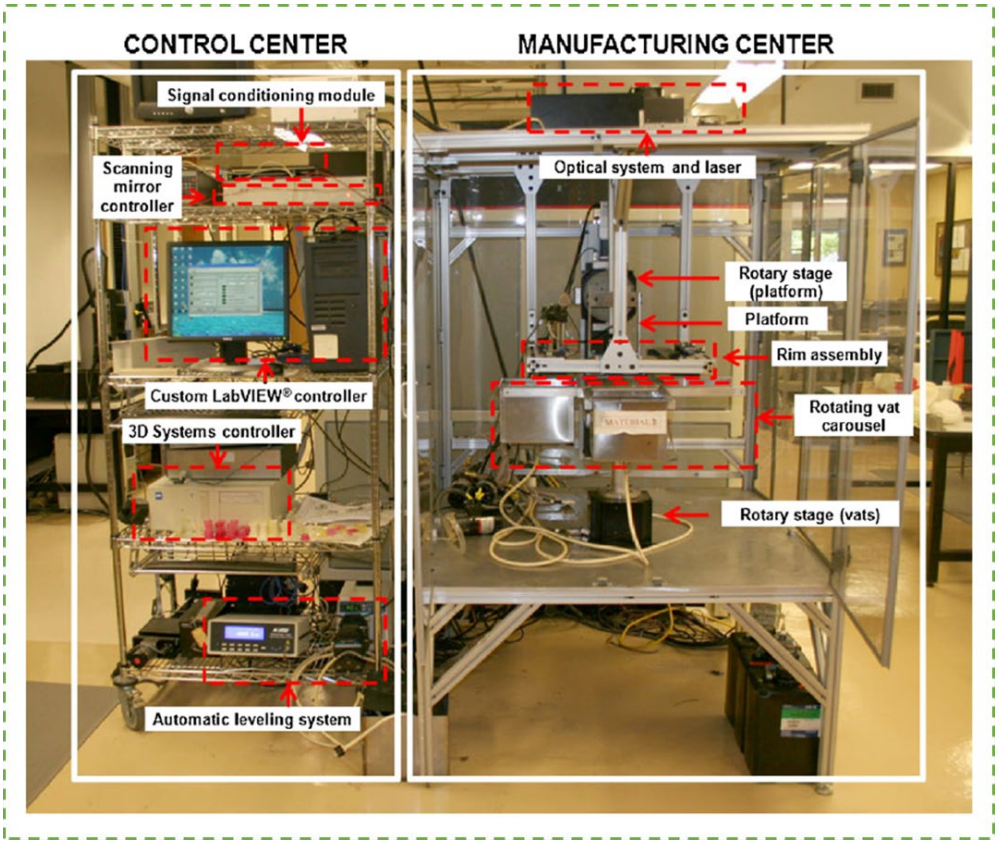

Figure 7: Developed MMSL machine.[38]

By installing parts from a 3D Systems 250/50 stereolithography (SL) machine on a different stand-alone system and converting the parts to work with extra parts necessary for MMSL operation, a multi-material stereolithography (MMSL) machine (Figure 7) was created. Building a new frame, rotating vat carousel system, platform assembly, and automatic leveling system were all necessary for the MMSL machine. The commercial SL control software (3D

Systems Buildstation 4.0) was retained for controlling the laser scanning procedure while a customized LabVIEW® program was used to manage the overall operation of the MMSL system, including maintaining a new vat leveling system and new linear and rotational stages. Due to the possibility of previously cured layers impeding the sweeping process during MMSL building, low-viscosity resins were employed in a deep-dip coating method rather than sweeping. Several multi-material complicated parts were created, offering convincing proof that MMSL can create one-of-a-kind parts that are functional, visually illustrative, and built with multiple materials.[38]

2.2 Electroplating

The technique of electroplating involves using electrolysis to cover a conductive surface with a thin layer of metal. It is primarily used to increase a surface's electrical conductivity, aesthetics, and corrosion resistance. The procedure entails adding a current to the system after dipping a conductive material, such as a metal, into an electrolytic solution. A thin coating of metal is deposited on the conductive surface because of the electrolyte solution's metal ions being drawn to it. Although electroplating provides several benefits, there are some drawbacks as well. The need for specialty tools, facilities, and chemicals is one of its key drawbacks. Moreover, it produces hazardous waste, which, if not handled and disposed of appropriately, can be bad for the environment. A further drawback of the electroplating process is that it can be rather expensive, particularly for small-scale manufacturing.[39] Semiconductors have been

deposited onto certain surfaces for a long time using the electrodeposition technique. Growing thin films and/or nanostructures with possible thermoelectric properties has shown to be a valuable use for this method. Electrodeposition has several advantages over physical processes, including its ability to operate economically and the availability of appropriate facilities.[40]

Electroplating on polymer substrates is a widely researched topic due to its potential applications in various industries. Electroplating on polymer substrates presents several challenges, primarily due to the non-conductive nature of polymers. Polymers such as polypropylene, polyethylene, and polycarbonate are widely used in industries such as automotive, aerospace, and electronics. However, these polymers cannot be electroplated directly due to their non-conductive nature. One of the most common methods to improve the electrical conductivity of polymer substrates is the deposition of a conductive layer. This conductive layer can be deposited using several techniques such as plasma treatment, chemical vapor deposition, and sputtering. To overcome this challenge, several methods have been developed to improve the electrical conductivity of polymer substrates. Several studies have been conducted to explore the potential applications of electroplating on polymer substrates. As conventional polymers are often insulators, changing their composition and structure necessitates either chemical or physical means. These indirect techniques involve several phases and are used in the electroplating process. Polymer surface activators, oxidizers, and etchants are extremely polluting and dangerous to human health. Chemical and physical processes, from an economic perspective, require highly specialized

equipment, which affects the final cost of the output.[41] Another method to improve the electrical conductivity of polymer substrates is the incorporation of conductive fillers. Conductive fillers such as carbon nanotubes, graphene, and silver nanoparticles have been extensively used to improve the electrical conductivity of polymer substrates. These fillers can be added to the polymer matrix during the manufacturing process, resulting in a conductive polymer composite. The addition of conductive fillers not only improves the electrical conductivity but also enhances the mechanical and thermal properties of the polymer composite. Once the polymer substrate is made conductive, electroplating can be performed using conventional electroplating techniques. The most common electroplating techniques used on polymer substrates are electroless plating and electrolytic plating. Electroless plating involves the deposition of a metal layer onto the polymer substrate using a chemical reaction, whereas electrolytic plating involves the deposition of a metal layer onto the polymer substrate using an electrochemical process.[42]

Results on the electroplating of poly(3,4-ethylene-dioxythiophene) were presented by Leeuw et al (PEDOT). PEDOT was chosen due to its high conductivity of roughly 300 S/cm and ease of processing in solutions. As a primer, N-(3-Trimethoxysilylpropyl) pyrrole is used to increase the adherence of PEDOT to glass substrates. Potentiation copper film deposition has taken place. It is demonstrated that a lateral propagation velocity known as the front velocity and an ongoing thickening velocity of already metalized regions accurately reflect the electrodeposit's thickness profile. The sheet resistance of the PEDOT films, as well

as the temperature, applied voltage, and composition of the electrochemical baths, have all been calculated as functions of the front velocity and uniformity. A straightforward mathematical model is used to understand the experimental data and characterize transitory thickening during electrodeposition on electrodes with high ohmic resistance. In perfect accord with theoretical predictions, it is discovered that the front velocity is related to the square root of the reciprocal sheet resistance.[43]

2.3 Principle & Methodology

Many different materials have been employed in some earlier research to boost the conductivity of heterogeneous resin to cover it with copper and produce characteristics akin to those of a scaly foot snail. The dynamic electrical field and stereolithography based on microscale mask image projection were combined in EFA-HMP. By using currently known methods, it is challenging to build metallic structures in a single step at ambient temperature. To preserve the transport of metallic ions and encourage metal deposition on the photocured polymer matrix, a composite made of a polymer matrix that may serve as an electrolyte was produced in this study. PEDOT: PSS and PEGDA were combined to improve the electrical conductivity of photocurable resin. In addition, the inorganic substances were included to supply adequate metal ions for the deposition.

The idea behind electroplating polymers is to use an electric current to transport metal ions from an electrolytic solution to the surface of a conductive polymer. The metal ions in the electrolytic solution serve as the anode and the

polymer surface as the cathode. The CAD model was first created and cut with the desired microstructures. The copper ion-containing photocurable polymer matrix solidified to create a two-dimensional (2D) pattern when a light beam was projected using the model's sliced pictures. It took several layers of this procedure for us to achieve the proper shape and size for the entire construction. The three-dimensional (3D) structure was created consisting of the 2D layers that were curing one after another. We were able to coat the printed polymer structure with the same resin that was used for printing since copper sulfate was present in the heterogeneous resin. We were able to research the deposition of copper onto various designs thanks to the study of microstructure. The concentration of metal ions, electrical field voltage, and deposition time all affect how metallic structures are formed. The process parameters were tuned based on physics-based modeling, simulation, and testing to accomplish precise printing of polymer/metal material systems with required geometric shapes.

Based on stereolithography, a brand-new 3D printing technique called Electrically Assisted Heterogeneous Material Printing (EFA-HMP) (Figure 8 a, b) was employed. A light source, such as a projector, and a guiding tool that serves as a build platform are crucial components of stereolithography printing technology. A tank containing photocurable liquid resin is immersed with the guiding instrument inside of it. Two copper electrodes that are facing one another and connected to an AC high-voltage source are placed in the vat tank. Because copper sulfate is present in the photopolymer resin, the electric field is employed to deposit copper on the 3D-printed structure. By combining dynamically controlled

laser beam projection with the single-axis movement of the guide tool, the EFA-HMP printing process may selectively solidify liquid resin to create microscale details on the surface of a macroscale item. Additionally, it enables us to print a structure and then selectively cover it.

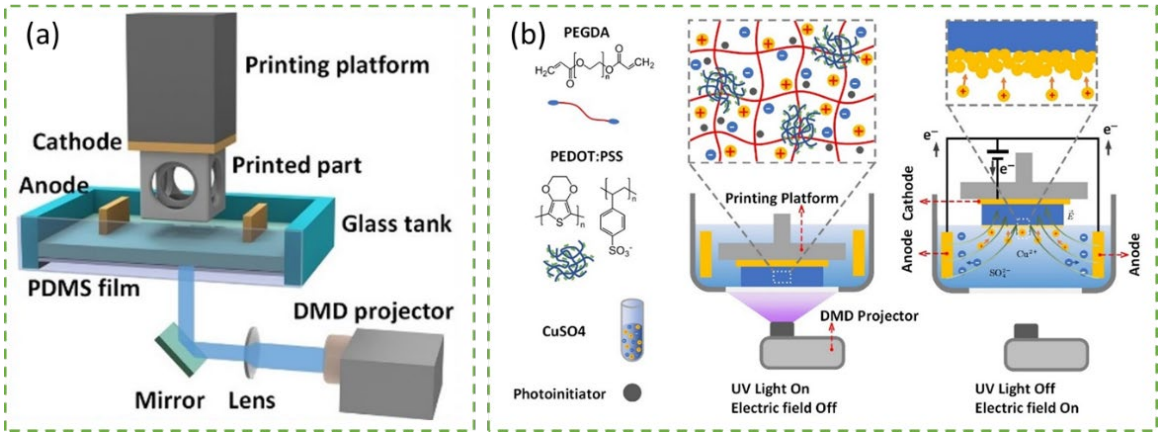

Figure 8: a) Illustration of optical projection and electrical field generation in the EFA-HMP. b) Schematic diagram of the curing process and electrical field-assisted metal deposition.

2.3 Problem Statement and Hypothesis

Obtaining anisotropic properties for a metal-polymer heterogeneous material system and understanding how the shape of the microstructure affects the deposition of copper onto a cured part using a recently developed photocurable electrolyte resin are the two main challenges involved in this research problem. The thesis puts forward the theory that the mechanical and electrical characteristics of the resulting composite material can be enhanced by a programmed distribution of metallic structures inside a polymer matrix. Additionally, it is proposed that altering the microstructures' morphology can control how the metal grows, improving the composite material's qualities overall.

CHAPTER 3 EXPERIMENTAL PROCEDURE

3.1 Material Preparation

A photocurable matrix and conductive fillers make up the photocurable electrolyte solution. The material used to make the photocurable resin were Poly (ethylene glycol) diacrylate (Mn 700) (PEGDA), Poly (ethylene glycol) diacrylate (Mn 250) (PEGDA), highly conductive poly (3, 4-ethylene-dioxythiophene)-poly (styrene sulfonate) (PEDOT: PSS) in the pure pellet with 3.0-4.0% H2O, and Irgacure 819 photoinitiator. Copper (II) sulfate (CuSO4) solution was made from crystals mixed with water with a concentration of 1 mol/L. Magnetic Stirring (Figure 9a), a method where the material is combined using a magnetic stirrer on an electromagnetic surface that rotates at high rates to create a rotating magnetic field and aid in the material's fast dispersion, was used to mix everything well.

Initially, PEGDA and PEDOT: PSS were utilized to create the photocurable matrix of the 3D printable conductive composite. To study the curing characteristics, and resistivity, 30 wt.% PEGDA 700, 10 wt.% PEGDA 250, and 2 wt.% Irgacure 819 photoinitiator were combined. The remaining fraction of the photocurable conductive resin was 1 mol/L CuSO4 solution dissolved using a varied ratio of the pellet formed PEDOT: PSS (1 wt.%, 1.5 wt.%, 2 wt.%, 2.5 wt.%, and 3 wt.%) by stirring at 200 rpm for 1 h at room temperature (25°C). The photocurable PEGDA matrix was then mixed with the conductive PEDOT: PSS fillers and the CuSO4 solution, and the mixture was agitated at 200 rpm for 8 hours at 25°C. To remove air bubbles from the resin, the prepared photocurable electrolyte solutions were

lastly degassed in a vacuum chamber. Microscopic images of the solution were captured to see the dispersion of PEDOT: PSS in the solution (Figure 9c). Following testing, the photocurable electrolyte solution (Figure 9b) used for printing and electrodeposition has been improved to contain 30 wt.% PEGDA 700, 10 wt.% percent PEGDA 250, 56 wt.% 1mol/L of CuSO4 solution, 2 wt.% of Irgacure 819 photoinitiator, and 2 wt.% PEDOT: PSS.

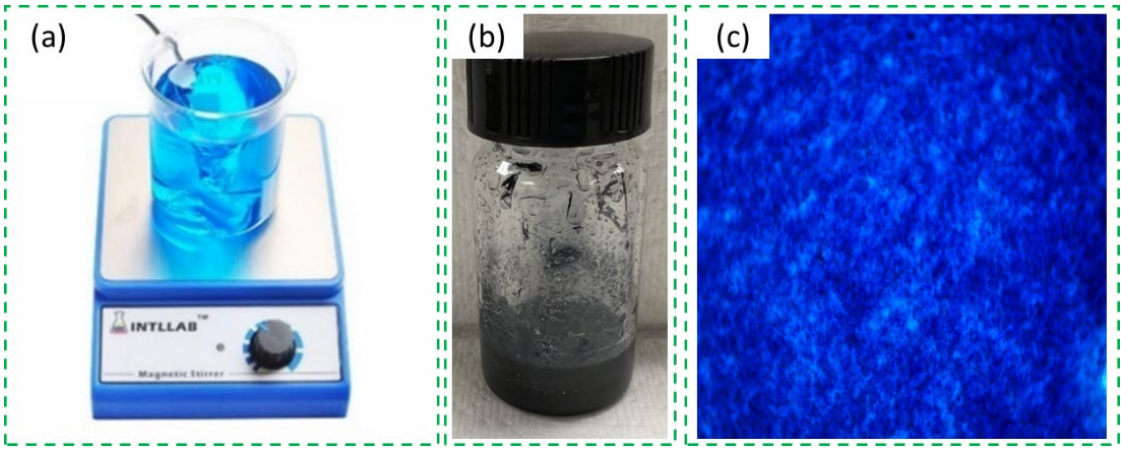

Figure 9: a) Magnetic Stirrer b) Photocurable electrolyte resin c) Dispersion of PEDOT: PSS in the heterogeneous mixture

3.2 Electrical field-assisted heterogeneous material printing

The experimental setup (Figure 10) comprises a specially constructed 3D printer configuration using a stepped motor, a controller, a UV light projector, and a unidirectional actuator. A unidirectional actuator is utilized for the z-axis moment since digital light projection 3D printing is a layer-by-layer technique. To regulate the rate of curing and the caliber of printing, the projector's light output is manually adjusted. A shutter blocker is connected to the stepper motor to reduce the amount of light the projector emits when printing. The computer is connected to the KFLOP controller, which is connected to the actuator and stepper motor. A power supply

is connected to the components indicated above. To control these devices, KMotion Software is employed. The 3D Lightyear program is used to change the size and location of the SolidWorks-designed CAD model in 3D space. When comparing the size ratio between the projected CAD model and the actual size of the printed item, the original CAD model is accurately updated in terms of dimensions and turned into an STL file. The KMotion Slicer Software is then used to slice this model horizontally for 50 m. As a result, the set of sliced photos utilized as masked images is required for printing. The number of photos obtained is entirely dependent on the CAD model's curing depth and the depth at which it was sliced. The CAD model's size is crucial since it can drastically alter the actual size of the printing structure. The structure is printed using all these photos, which are kept in a folder and printed one after the other.

One at a time, the projector projects the sliced images onto the vat tank's bottom surface. The vat tank is anchored in every direction to avoid any movement. The printed constructions could lose the required shapes and qualities if the vat tank is not firmly fastened in situ. Also, this changes the focus and printing resolutions of the projector, which could lead to distorted shapes and poor print quality. The flat guiding tool is set such that there is some resin between its lowest point and the tank's bottom surface so that the UV lights can cure a layer and print it on the flat tool. The programming software regulates the exposure time, the number of layers to print, the travel distance of the flat tool, the layer thickness, and the projected images. As a result, after the initial picture is projected into the photopolymer resin, the first layer is printed on the flat tool's bottom surface. The

flat tool is then elevated to form a new layer based on the set layer thickness and lowered in a regulated motion to allow extra resin in between the subsequent layers. A structure is then printed after several iterations. The UV projector emits images that are illuminated by bright light. The light is blocked by a shutter coupled to a stepping motor to avoid over-curing between the various layers. It is set up to open when the projected image appears and to close based on the exposure time that follows. How quickly the flat tool raises and lowers for each print is determined by the controlled speed, which is based on the number of layers to be printed. For each projected image, the flat tool is elevated 50 times at a thickness of 100 micrometers, or 5000 times at a speed of 100 micrometers per second. By doing this, it will be possible to control the structure's shape during printing and elevate the printed layers wit Printing speed and layer depth both influence how rough the print's surface is. Like other 3D printing techniques, slower printing speeds improve the structure's shape. The layer depth and exposure time are completely influenced by the mixture and its curing characteristics. After printing is complete, the printed object is cleaned with isopropyl alcohol to remove any extra resin before being dried. The same photocurable electrolyte solution is then used to deposit copper into the microstructure of the printed pieces. The preprinted portion was lifted to form metallic structures by ensuring that only the surface that needed metal deposition was in contact with the solution. The entire printed component then functioned as a cathode after the electrical field was activated. In the meantime, the glass tank had two copper electrodes (20 mm and 50 mm) that were activated as anodes for upcoming electrodeposition. Copper ions were continually

produced by the anode during electrodeposition, and the copper ions traveled to the polymer matrix's surface to pick up electrons and form copper particles.

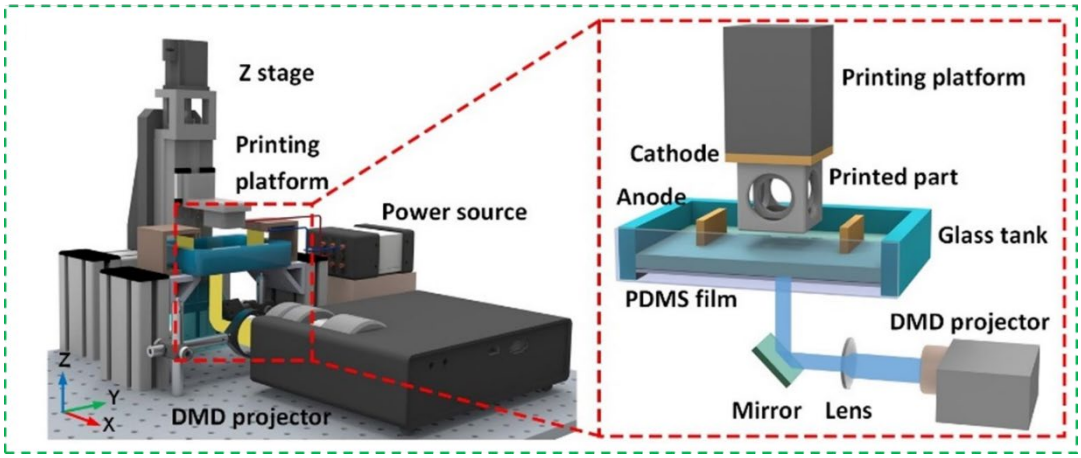

Figure 10: Schematic diagram of the EFA-HMP set-up

3.3 COMSOL simulation of metal deposition under electrical field

In the manufacturing sector, electrodeposition is a frequently used technique for depositing a metal or alloy on a substrate using an electrolytic solution. To deposit the metal ions into the substrate, the method entails applying an electric potential across an electrode submerged in an electrolytic solution. An efficient technique to streamline the procedure and raise the caliber of the deposited layer is to simulate the electro-deposition process. With the help of the powerful software program COMSOL Multiphysics, the electro-deposition process was more precisely simulated. The simulation was based on the electrochemistry principles, which describe how ions and electrons move through an electrolytic solution. A two-dimensional model of the simulation will consider the impacts of the electrode geometry, the make-up of the electrolytic solution, the passage of

time, and the applied voltage. Using experimental data gathered from a genuine electro-deposition process, the model will be verified.

The model decides to use COMSOL Multiphysics to simulate the deposition process at pH 4 to lessen the impact of proton concentration on copper deposition under the electrical field. Because of this, it is not necessary to represent the mass balance of protons, and sulfate is likewise treated as a free ion. As the model entirely rules out any potential side reactions and there is no charge loss, we assumed that the occurrence rates of deposition at the cathode and dissolution at the anode are 100%. During the metal development, there is a difference in the electrolyte density, which causes the anode to have a higher density than the cathode. Free convection can be disregarded, though, because little will change in the components under the circumstances of this modeling. The simulation findings show that the cathode border will shift as the metal is deposited, demonstrating that the metal deposition process is essentially time-dependent. As a result, throughout the deposition process, the cathode surface is tracked using the Level-Set interface, which also automatically creates the interface motion equation between the liquid electrolyte and the solid electrode. Although if PEDOT: PSS exists in the form of solid particles that are conductive fillers, their impact on the mobility of copper particles can be disregarded. The simulations were conducted for various cases of microstructure with varying shapes and sizes and time. For ease of use, the electrolyte solution is made from a 1:1 mixture of PEGDA and 1 mol/L $CuSO_4$ solution. To assess the effects of the printed part's geometry on the

metal growth and deposition, the metal deposition on flat surfaces with and without a bump was simulated. Some parameters used in the simulation were as followed.

- Initial concentration 500 mol/m^3
- System temperature 298 K
- Exchange current density 150 A/m^2
- Anode potential 0.135 V
- Cathode potential -0.135 V
- Diffusivity, species Cu 2e-9 m^2/s
- Molar mass of copper 0.06355 kg/mol
- Density of copper 8960 kg/m^3

To ascertain the effects of the different parameters on the caliber of the deposited layer, the simulation results will be examined. The accuracy of the simulation model will be confirmed by comparing the simulation results with experimental data. The simulation findings will offer perceptions into the electro-deposition process optimization, and the outcomes can be used to build electro-deposition procedures that are more effective.

3.5 Electrical Conductivity

A material's ability to conduct electricity is described by its electrical conductivity, which is a fundamental attribute of materials. It is a crucial characteristic that is utilized in many fields, including electronics, power production, and energy storage. On the other hand, a multimeter (Figure 11) is a device used to gauge a material's electrical characteristics. Voltage, current, and resistance

measurements can all be made using it. To model electrical conductivity with COMSOL, the material's design must first be established. The geometry can be generated with COMSOL's built-in CAD tools. We then apply the proper boundary conditions to the model once the geometry has been established. To see how electric current flows across copper deposits and how different designs and amounts of copper deposited will alter the flow of current, voltage is applied across the junction where copper is deposited.

Figure 11: VC830L Multimeter

Further with the suitable COMSOL material model, the material properties are specified. The conductivity, resistivity, and other electrical characteristics of the material will be described in the material model. We solve the model using COMSOL's FEM solver after defining the geometry, boundary conditions, and material properties. As a function of the applied voltage, the solver will determine the current density and electric field distribution in the material. Calculating the

material's conductivity and resistivity is possible using the simulation's results. Connecting the material to the multimeter and measuring its voltage, current, and resistance are the steps in physical measurement. Calculating the material's conductivity and resistivity is possible using the measurement findings. The electrical conductivity of the material under various conditions can be predicted using the simulation's findings. The conductivity and resistivity of the material can be determined using the simulation, as well as any potential weak spots in the material. A practical way to determine a material's electrical conductivity is through physical measurement using a multimeter. The measurement can be used to validate the simulation's correctness and to confirm the outcomes of the simulation.

3.4 COMSOL Simulation of Mechanical performance

A primary technique for figuring out a material's mechanical properties is tensile testing. It entails placing a controlled tensile load on a specimen while observing how the material responds to stress and deformation. The results of this test can be used to evaluate a material's strength, ductility, and toughness. Numerical simulations are now a valuable tool for studying and forecasting the behavior of materials under tensile loading because of technological advancements. A potent piece of software called COMSOL Multiphysics may be used to simulate and examine the behavior of materials under various loading scenarios. The governing equations of a problem are solved using the finite element method (FEM).

We first specify the specimen's geometry in COMSOL to simulate a tensile test. The specimen's geometry is constructed using the CAD tools incorporated into COMSOL, and the tensile test bar is designed per ASTM standards. For the simulation of the tensile test, the geometry is created using tensile test specimens of various shapes and sizes, as well as copper that has been deposited at various copper thicknesses. We apply the proper boundary conditions to the model once the geometry has been established. The top end is where the force is applied; the bottom end is where the force is fixed. The specimen's material characteristics must then be defined. With the suitable COMSOL material model, the material properties may be specified. The elastic modulus, Poisson's ratio, and density of the material will all be specified by the material model. The properties used for the simulation were.

PEGDA

- Density- 1120 kg/m3
- Young's Modulus- 8.3e7 pa
- Poisson's ratio- 0.3

Copper

- Density- 8960 kg/m3
- Young's Modulus- 1.3e11 pa
- Poisson's ratio- 0.34

When the geometry, boundary conditions, and material characteristics are established, we use COMSOL's FEM solver to resolve the model. As a result of

the applied load, the solver will determine the specimen's stress and strain distribution. The stress-strain curve of the material, which is a fundamental characteristic that characterizes the mechanical behavior of the material, can be calculated using the simulation's results. The simulation's findings can be used to forecast how the material would behave mechanically under various loading scenarios. The simulation can also be used to pinpoint possible weak places in the material and evaluate the effects of various factors on the material's mechanical behavior.

CHAPTER 4 RESULTS AND DISCUSSION

4.1 Curing characterization of printing material

The amount of time required for the photopolymerization of the polymer resin into a solid material is known as the curing time. The substance used affects how quickly or slowly the resin cures. To gain a basic understanding of the impact of fillers on the curing of polymer-based solutions, the curing characteristics of the photocurable electrolyte solution containing 2 wt.% of PEDOT: PSS were investigated. The PEDOT: PSS fibers are dispersed evenly across the PEGDA matrix. To solidify a specific area, the 2D light pattern is projected onto the surface of the solution. The relationship between light penetration, volume percentage, and total energy was devised to determine the cure depth Cd of the photocurable resin. The curing model of MWCNT-based resin during the e-VPP procedure could be predicted using the equation derived by Griffith and Halloran [44] as follows:

$$C_d = \left(\frac{\eta_0}{\eta_P - \eta_0}\right)\frac{\lambda^2}{D}\ln\left(\frac{t}{t_c}\right)\frac{1}{\phi}$$

where λ is the wavelength of light in nm, D is the diameter of the PEDOT: PSS particles, t is the exposure duration, t_c is the critical exposure time, and φ is the concentration of PEDOT: PSS particles. η_0 is the refractive index of the photocurable PEGDA resin. η_P is the refractive index of the PEDOT: PSS. The curing study was done for different layer thicknesses under UV light. The UV projector with a resolution of 7.6 μm was used to cure a layer of thickness 0.1mm, which took 7s.

4.2 Microstructure design

To study the deposition of copper onto the structures made of photocurable electrolyte solution microstructures were introduced to study the effect of various shapes on deposition. The 3D Lightyear program is used to change the size and location of the SolidWorks-designed CAD model in 3D space. When comparing the size ratio between the projected CAD model and the actual size of the printed item, the original CAD model is accurately updated in terms of dimensions and turned into an STL file. The KMotion Slicer Software (Figure 12d) is then used to slice this model horizontally. As a result, the set of sliced photos utilized as masked images is required for printing. The number of photos obtained is entirely dependent on the CAD model's curing depth and the depth at which it was sliced. The CAD model's size is crucial since it can drastically alter the actual size of the printing structure. The structure is printed using all these photos, which are kept in a folder and printed one after the other. After being divided into slices for VPP 3D printing, the pictures are projected one at a time from the projector onto the bottom surface of the vat tank. A collection of sliced photos (Figure 12e) that are saved in a folder are used by the application that projects these masked images onto the bottom surface of the vat tank. The vat tank is anchored in every direction to avoid any movement. The flat guiding tool is set such that there is some resin between its lowest point and the tank's bottom surface so that the UV lights can cure a layer and print it on the flat tool. The programming software regulates the exposure time, the number of layers to print, the travel distance of the flat tool, the layer thickness, and the projected images. As a result, after the initial picture is projected into the

photopolymer resin, the first layer is printed on the flat tool's bottom surface. The flat tool is then elevated to form a new layer based on the set layer thickness and lowered in a regulated motion to allow extra resin in between the subsequent layers. A structure is then printed after several iterations. The UV projector emits images that are illuminated by bright light. As a result, the photopolymer might over-cure. So, the intensity of the UV projector is kept at 30% only.

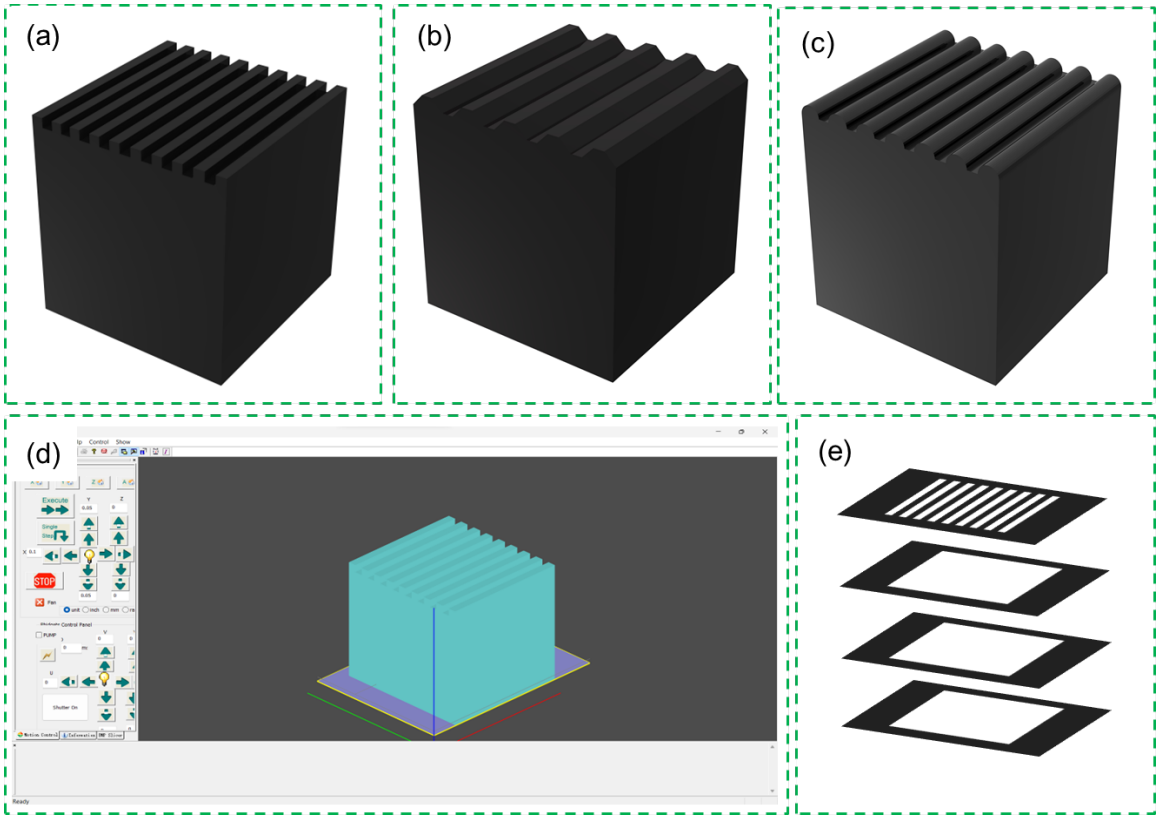

Figure 12: a) CAD Model of Cube with rectangular microstructure b) CAD Model of Cube with trapezium microstructure c) CAD Model of Cube with semicircle microstructure d) Slicing Software e) Projection images.

In this thesis, the study was conducted for 3 different microstructures and each cad model was designed to its specifications. The structures that were selected to be made at the bottom of the cube were a rectangular shape (Figure

12a), a trapezium (Figure 12b), and a semi-circle (Figure 12c). For the rectangular shape, the cad model was sliced for 100 microns per layer whereas for the trapezium shape at the bottom, the cad model was sliced for 50 microns per layer to achieve the proper shape of the microstructure and for the semi-circle shape at the bottom the cad was sliced for 35 microns per layer. For all the cubes the total height was kept at 0.5mm whereas the microstructure was 400 microns in height. The final printed cube was 6.1mm in length and 6.4mm in breadth with the microstructures printed along the length.

4.3 Modeling of metal growth on 3D printed microstructures.

Further investigation was conducted on the formation of metallic structures after investigating the ability of the printing electrolyte solution to cure. To investigate the viability and efficiency of the metal deposition under the electrical field using the photocurable electrolyte solution suggested in this thesis, the fabrication performance of metallic structures using EFA-HMP was quantitatively evaluated by calculating the thickness of the deposition, which is discussed in this section. Electrical field-assisted metal deposition on the photocurable electrolyte solution shows a high correlation between deposition thickness, electrical charge, and deposition time. Studies were conducted for various voltages and times on a thin film to monitor the deposition of copper (Figure 13a). To investigate the quality of metallic structures printed by the EFA-HMP technique, a physics-assisted simulation was carried out. A range of voltages between 50V and 100V was employed in the studies to determine the link between deposition thickness and

various voltages for a set time of 5 mins. When a 50V voltage is used, the copper deposition thickness after 5 minutes can reach 3μm. To constantly start the electron, transfer necessary for electrical field-assisted metal deposition to produce a thicker coating, there was not enough potential difference. Yet, the thickness of copper that was deposited dramatically increased as the applied voltage crossed a particular threshold. For instance, when the deposition duration was 5 minutes, the copper deposition thickness increased from 8μm at 60V to 51μm at 80V (Figure 13b).

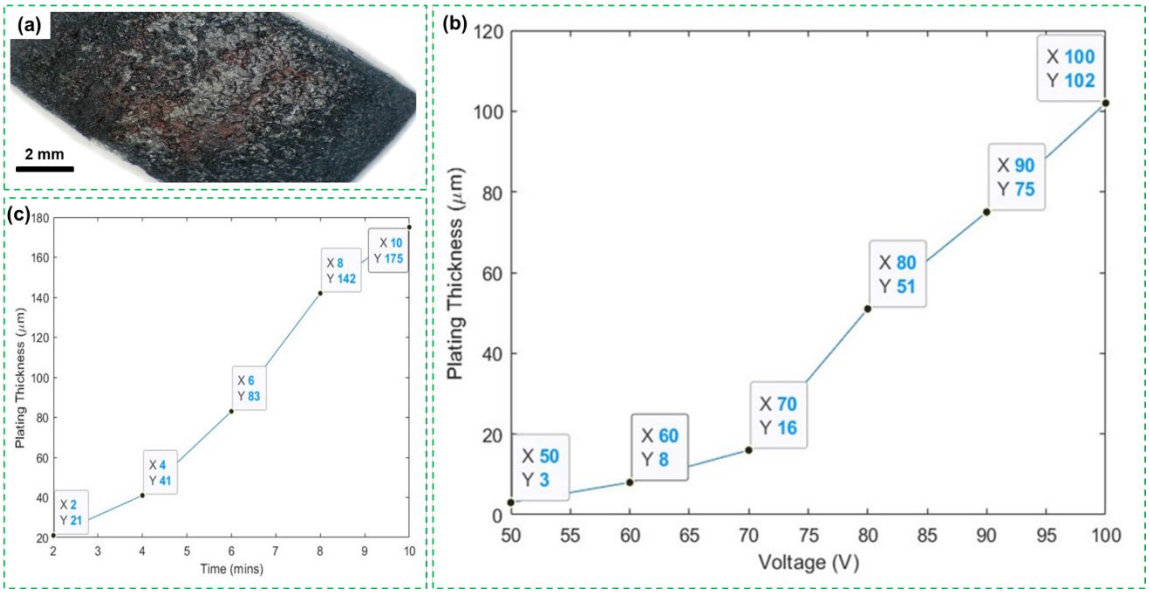

Figure 13: a) 3D Printed thin film with copper coating b) Plating Thickness after 5 mins Vs Voltages c) Plating thickness at 80V Vs Time

Yet, the too-high voltage will have adverse consequences that electrolyze the water in the solution, and this response is what matters most. This is because the copper cations' Cu^{2+} movement speed in the high-viscosity solution is constrained. The cured component will also progressively start to lose water and have its conductivity reduced by the heat produced during the electrical field-

assisted metal deposition process, which prevents it from supporting metal deposition. The thickness of copper at various depositing times under 80V was experimented with in terms of deposition time. In 2 minutes, the thickness was 21μm, and at 10 minutes, it was 175μm (Figure 13c). After 10 minutes, however, the thickness remained constant, and the produced copper particles were dissolved in the printing solution close to the deposition area. This is due to the pre-deposited copper coating on the hardened polymer component making it difficult for the newly deposited copper particles to adhere.

4.3.1 Simulation

COMSOL Multiphysics was used for the simulation. Several designs, including rectangular, trapezoidal, and semicircular microstructure forms, were simulated. Each simulation was run many times for time intervals ranging from 1 to 9 seconds at a 2-second interval. The COMSOL CAD designer was used to build a total of 9 unique and distinct designs that were then simulated for electro-deposition. According to the simulation results, as can be seen from the brown area, a thin, homogeneous layer of copper particles progressively forms on the pre-cured polymer-based component. This layer is exposed to an electric field. The thickness of the plating layer gradually increases over time, according to the modeling of the developing process of the metallic structures on the flat surface plating. It was assessed how well metallic structures with complicated 3D shapes, such as semicircular, trapezoidal, and rectangular microstructures, could be formed. The dimension of the domain was set as 2X3mm for all the simulations and the microstructures were uniformly distributed in the domain. Due to the

uneven coating thickness, it was discovered that the top surface of the microstructure was thicker than the others. The distribution of the electric potential will be directly impacted by the unevenness formed by the metallic structures on the microstructure, which will further reinforce the growth's non-uniformity. As a result, it is necessary to modify the deposition time during the printing of the metal layer to manage the uneven growth of the metallic structures. A large shift in the concentration of copper cations Cu^{2+} in the solution close to the deposition area is also indicated by the simulation findings, which is consistent with the number of copper particles deposited on the surface. The simulation results were used to understand the deposition of copper onto microstructures.

In the first test case, three rectangular microstructure designs were created, all with the same overall domain but varying in length and width. In the first case, the length and width of the microstructure were equal (Figure 14a). As time progressed, the thickness of the deposited copper increased, starting at the walls of the microstructure. At t=1s, uneven deposition of copper was observed on the microstructure walls. By t=7s, the microstructures were completely covered with deposited copper, with higher concentrations of copper at the center and lower concentrations at the far ends. In the next case, the length of the microstructure was twice that of the width (Figure 14b), and in the third case, the width was twice the length (Figure 14c). The deposition of copper particles over time followed the same trend for all three designs. However, the only notable difference was the formation of bumps and the convexity of the same due to the inability of copper ions to adhere to pre-deposited copper effectively.

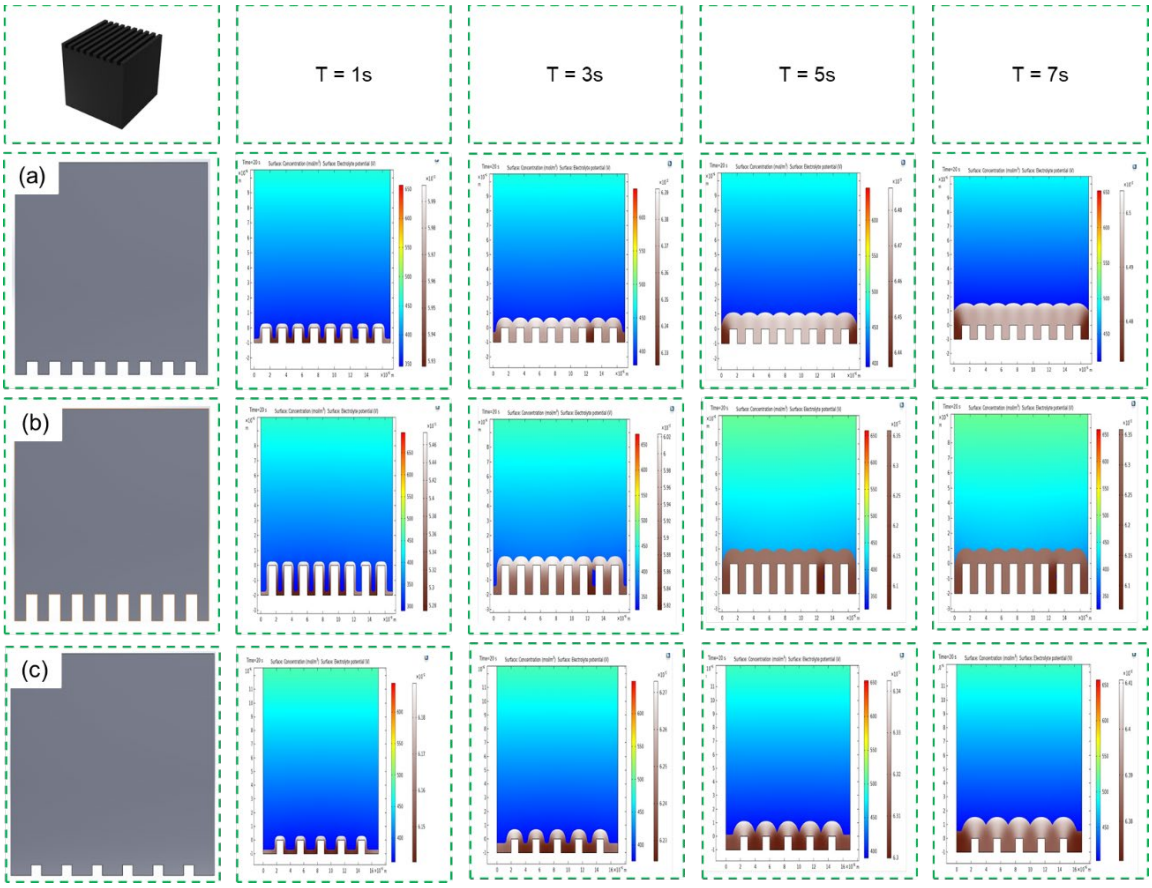

Figure 14: Simulation of metal deposition under the electrical field. a) length and width of the microstructure equal b) the length of the microstructure is twice of width c) the width of the microstructure is twice the length.

In the second test case, three semi-circular microstructure designs were created, varying in the radius of the semi-circle compared to the gap. For the first design, the radius of the semi-circle was half of the gap (Figure 15a), while in the second, it was twice the gap (Figure 15b). In the third design, the radius of the semi-circle was equal to the gap (Figure 15c). Like the first test case, as time progressed, the thickness of the deposited copper increased, starting at the walls of the microstructure. Even deposition of copper was observed on the microstructure walls at t=1s for all three designs. By t=7s, the microstructures were completely covered with deposited copper, with higher concentrations of copper at

the top and lower concentrations near the microstructures. The deposition of copper particles over time followed the same trend for all three designs, but there was a notable difference in the depth of the troughs at t=7s. In particular, the troughs in Figure C were much deeper compared to the other test cases.

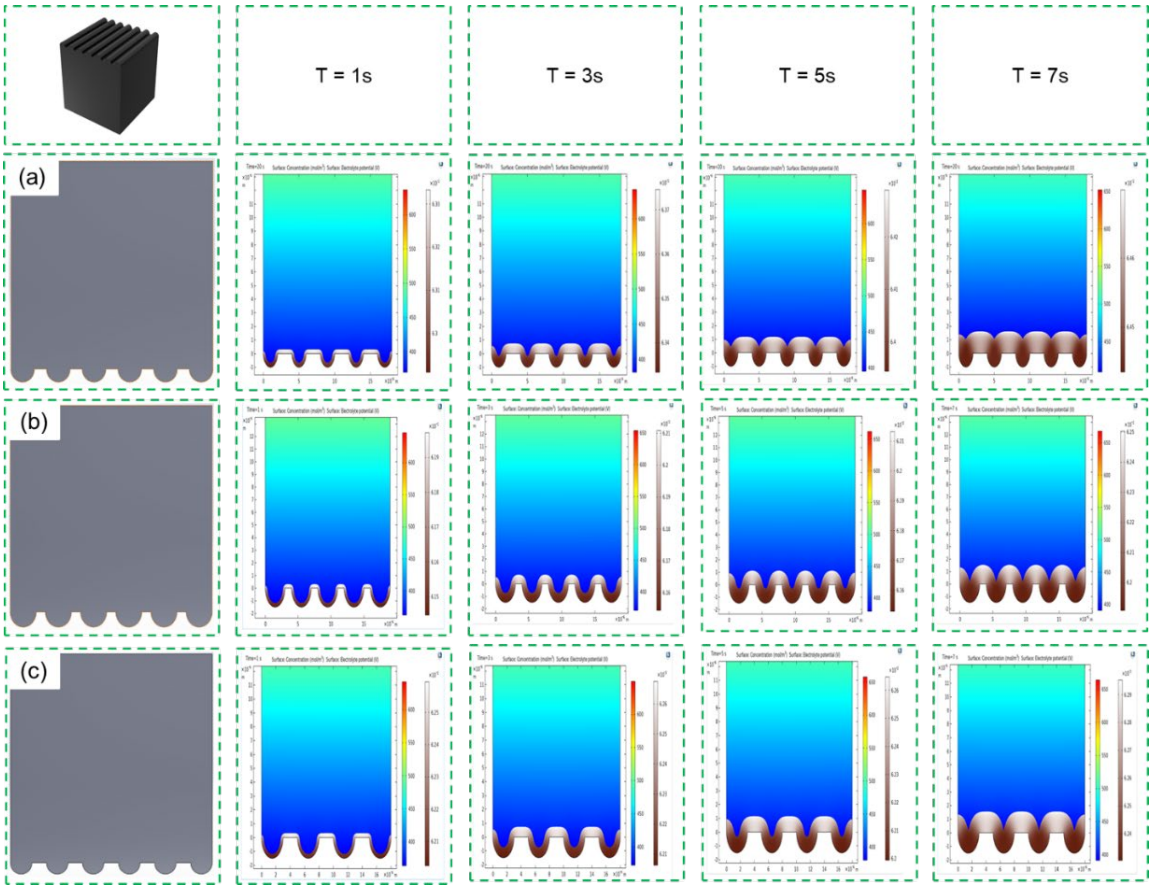

Figure 15: Simulation of metal deposition under the electrical field. a) the radius of the semi-circle is half of the gap b) the radius of the semi-circle is twice the gap c) the radius of the semi-circle is equal to the gap.

In the third test case, three trapezium-like microstructure designs were created, varying in the bottom length of the trapezium compared to the gap. In the first simulation, the bottom length of the trapezium was equal to the gap (Figure 16a), while in the second simulation, it was twice the gap (Figure 16b). Third, the bottom length of the trapezium was half the gap (Figure 16c). Like the previous

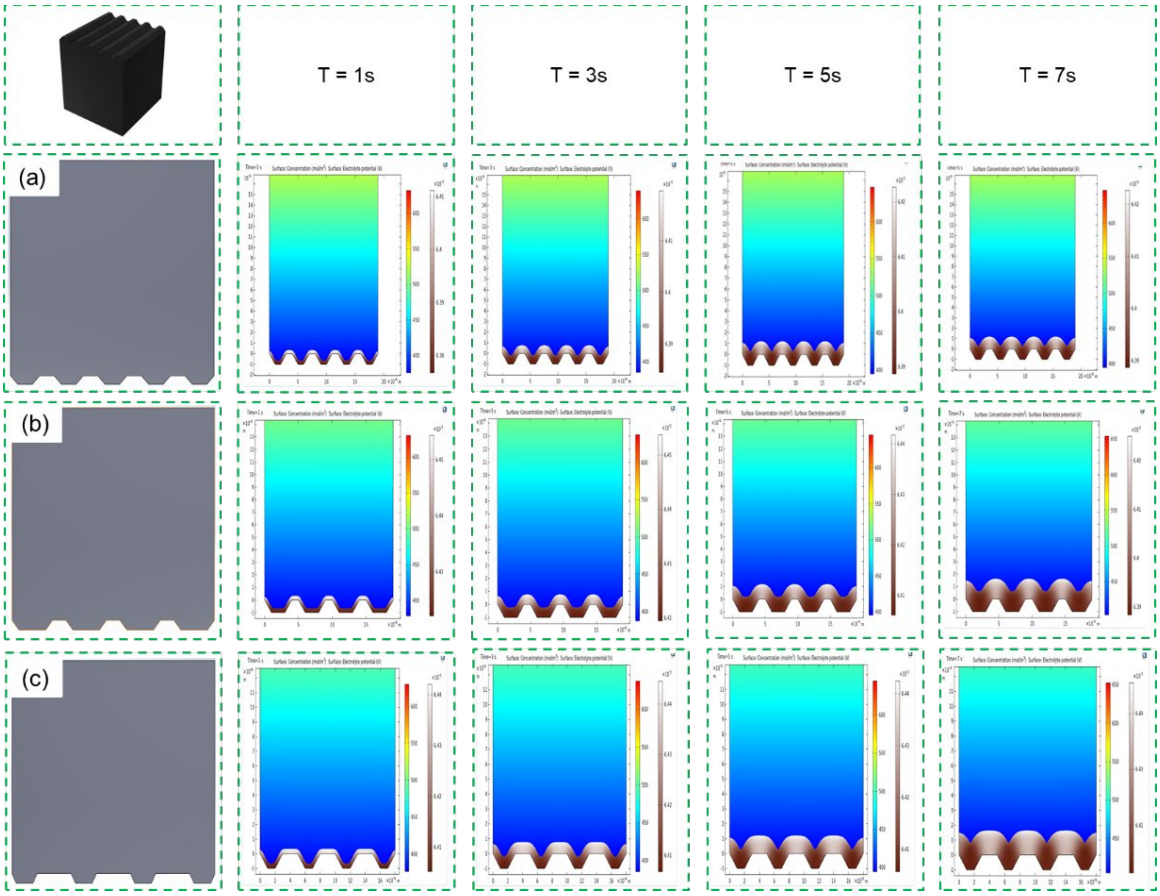

Figure 16: Simulation of metal deposition under the electrical field. a) the bottom length of the trapezium is equal to the gap b) the bottom length of the trapezium is twice the gap c) the bottom length of the trapezium is half the gap.

test cases, the thickness of the deposited copper increased as time progressed, starting at the microstructure walls. Even deposition of copper was observed on the microstructure walls at t=1s for all three designs, and by t=7s, the microstructures were completely covered with deposited copper, with higher concentrations at the top and lower concentrations near the microstructures. The deposition of copper particles over time followed the same trend for all three designs, but the only notable difference was the formation of bumps and the convexity of the microstructures. However, the number of bumps in this test case was significantly less compared to the first test case.

4.3.2 Physical test

The experiments conducted on the photocurable electrolyte solution, aided by an electrical field, revealed a strong correlation between the thickness of the deposition, the electrical charge, and the deposition time. To study the relationship between deposition thickness and different voltages, the experiments used a range of voltages from 50V to 100V. The results showed that there was not enough potential difference to initiate the electron transfer necessary for thicker coating at a constant rate. However, the thickness of the copper deposition significantly increased as the applied voltage crossed a certain threshold. After conducting various tests on a thin film, the deposition voltage was set at 80V. The 3D-printed cubes, measuring 5mm in height, were printed using the photocurable electrolyte resin. After printing, the cubes were immersed in copper sulfate solution to keep them wet as the electrical conductivity of the material decreased significantly after drying. Each test case involved electroplating the cube for 12 minutes at 80V in intervals of 4 minutes. This was necessary as the heat generated during the electrical field-assisted metal deposition process gradually made the cured part and the solution loses water, thus reducing their conductivity and preventing further deposition.

The first specimen shows the side and top view of the cube printed with rectangular microstructure (Figure 17a), and it can be observed that deposition occurred only between the microstructures, as the top part was smooth and did not allow copper particles to adhere. Whereas the second specimen shows the side and top view of the cube with trapezoidal microstructures (Figure 17b), and

the copper deposition was better on this cube due to the reduction of layer breadth during the printing process, which resulted in a rougher surface and better deposition results.

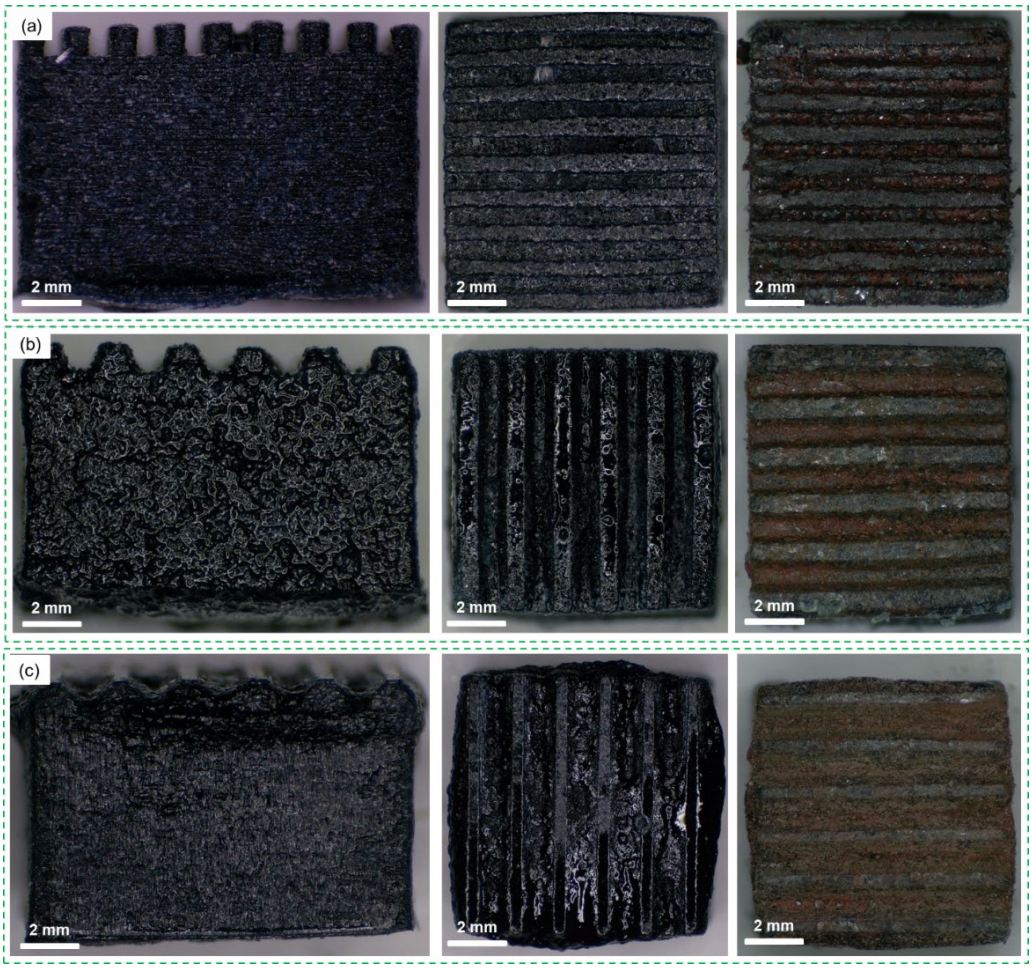

Figure 17: Top and side view of the microstructure with deposition results of a) rectangular microstructure b) trapezoidal microstructure c) semicircular microstructure.

The third specimen shows the side and top view of the cube with semi-circular microstructures (Figure 17c), and the copper deposition on this cube was the best of the three designs. This was due to the greater reduction of layer breadth during the printing process, resulting in a rougher surface and better deposition results. In all three cases, the deposition occurred between the gaps of the

microstructures, and the simulation results showed that the best deposition results were obtained with the semi-circular pattern.

4.3.3 Microstructure Evaluation

An effective imaging method used to examine the surface appearance and structure of various samples is scanning electron microscopy (SEM). It functions by scanning a sample's surface with an electron beam to provide high-resolution pictures of the sample's topography. In conjunction with scanning electron microscopy (SEM), the analytical method known as energy dispersive X-ray spectroscopy (EDS) can reveal a sample's constituent makeup. As an electron beam interacts with the atoms in the sample, distinctive X-rays are created that can be detected by EDS. The elemental makeup of the sample is then determined by analyzing these X-rays. The procedure of using both scanning electron microscopy (SEM) and energy dispersive X-ray spectroscopy (EDS) to examine the surface morphology and components of a part after copper deposition was carried out. These two methods were used to compile a thorough examination of the part's surface characteristics and chemical composition.

For the first test, a cube with rectangular microstructures was used, and the upper part of these microstructures were the focus of the microscopy and spectroscopy. With a focus on the region of copper deposition, this method enabled a targeted study of the sample's surface characteristics and chemical composition. The upper surface of the cube showed the presence of copper, sulfur, oxygen, and carbon, per the EDS findings (Figure 18a). Unevenness and cavities in the structure were discovered through additional SEM investigation of the

surface morphology of the rectangular microstructures (Figure 18b). Zooming in revealed the crystal structures of the deposited copper. The gap region was less obvious in the EDS data than the upper section of the microstructures because of the consistency and depth of the gaps.

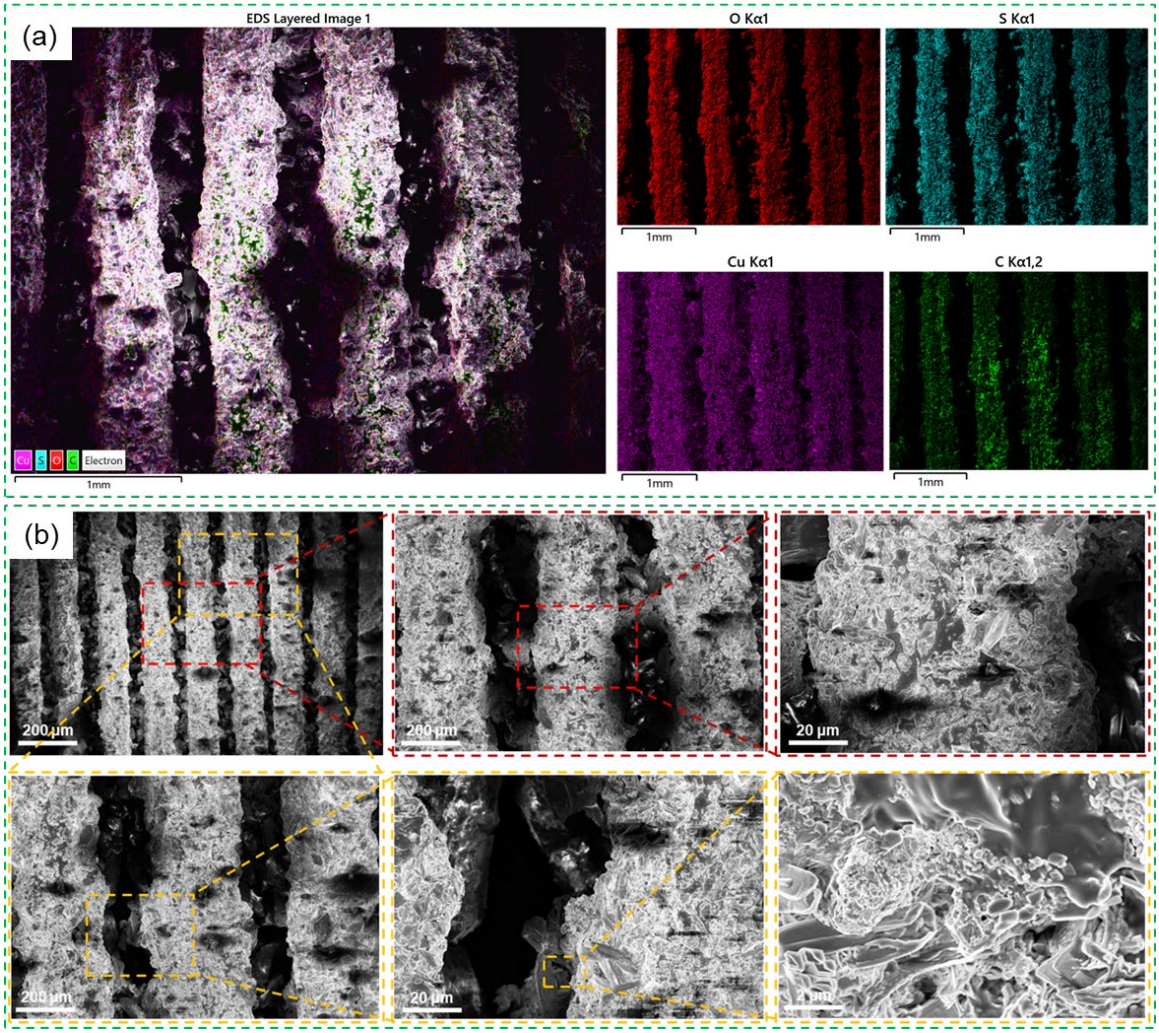

Figure 18: Top View of Rectangular Microstructure after Deposition a) Energy dispersive X-ray spectroscopy b) Scanning Electron Microscopy

In the second test, SEM and EDS were used to assess trapezoidal microstructures. The analysis's focus on the copper-deposition region made it possible to examine the sample's surface characteristics and chemical make-up

with precision. The microstructures' upper surfaces were found to include copper, sulfur, oxygen, and carbon, with more copper being present than in the first case, according to the EDS data (Figure 19a). A deeper SEM investigation of the surface morphology of the trapezoidal microstructures revealed less voids and irregularities, which can be attributed to the sample's printing process's reduced layer thickness (Figure 19b). Zooming in revealed a denser network of crystal formations.

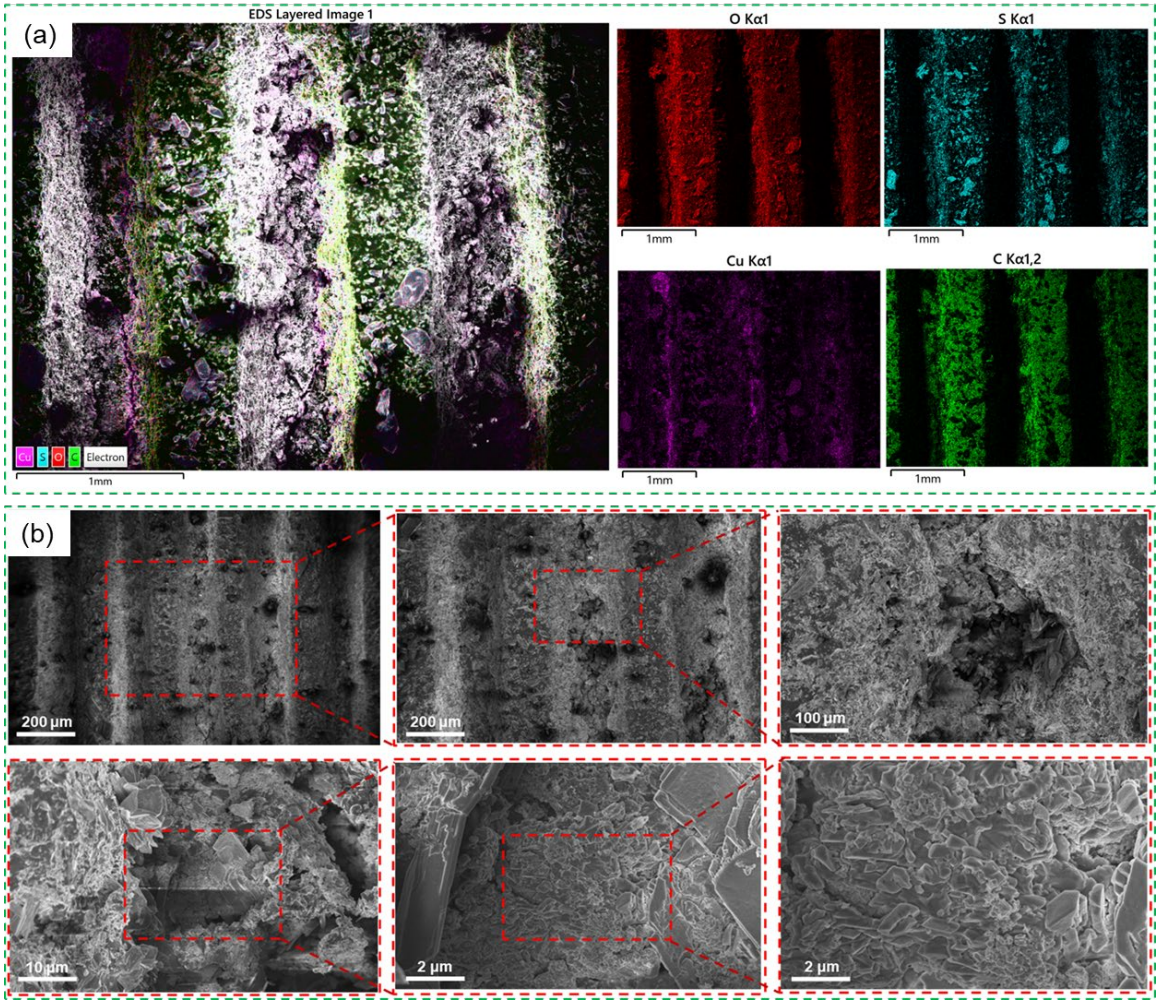

Figure 19: Top View of Trapezoidal Microstructure after Deposition a) Energy dispersive X-ray spectroscopy b) Scanning Electron Microscopy

Contrary to the first instance, the distance between succeeding gaps was greater, vividly highlighting the gap section in both the EDS and SEM data.

The third test employed semi-circular microstructures for the same evaluation procedure. The EDS results, which showed the deposition of all other substances as well as a higher amount of copper between the gaps, further validated this test's highest deposition performance among the three examples (Figure 20a).

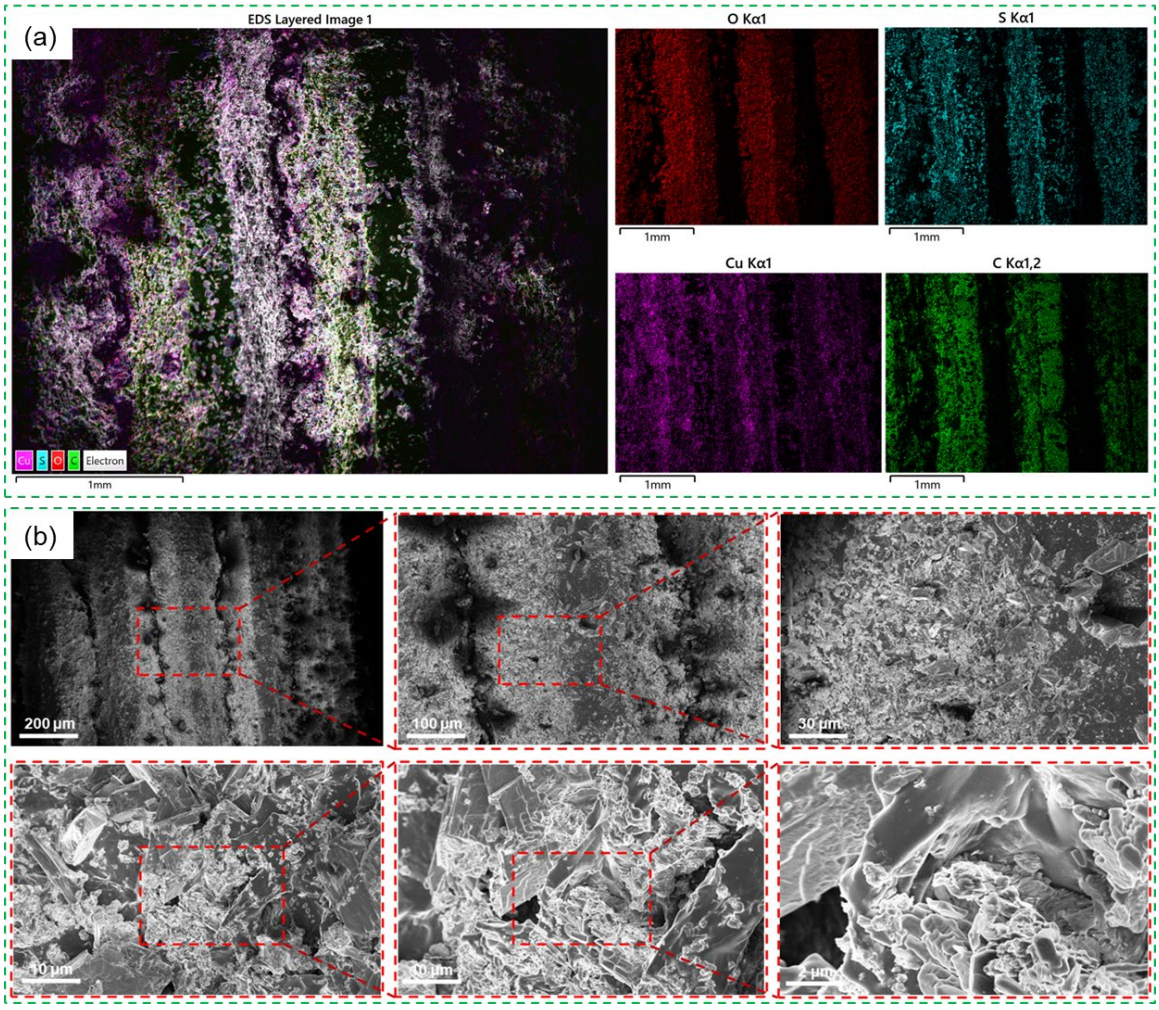

Figure 20: Top View of Semi-Circular Microstructure after Deposition a) Energy dispersive X-ray spectroscopy b) Scanning Electron Microscopy

Due to the utilization of the thinnest layer thickness during printing, SEM inspection of the surface morphology of the microstructures revealed nearly no voids and a better packed structure (Figure 20b). In contrast to the other cases, the surface also showed a richer crystalline structure, which was even more obvious when zoomed in.

4.4 Modelling of Electrical conductivity with metallic and polymer microstructures

The electrical conductivity of metallic and polymer microstructures is a crucial property that has been extensively studied for various applications in fields such as electronics, energy storage, and sensors. Modeling this property accurately is essential to optimize the performance of metallic and polymer microstructures. In metallic microstructures, the electrical conductivity is influenced by factors such as the material properties, the microstructure geometry, and the fabrication method used. By accurately modeling these properties, we can predict the conductivity and resistivity of the material and identify any potential issues that may arise under different conditions. These simulations, when combined with physical measurement, can provide a comprehensive understanding of the material's electrical characteristics, which is invaluable for numerous applications in industry and research. One such example of a conductive polymer mixture is PEDOT: PSS. It is composed of two ionomers, one of which is sulfonated polystyrene and the other is a conjugated polymer based on polythiophene, known as poly(3,4-ethylene dioxythiophene) (PEDOT). These charged macromolecules

form a macromolecular salt and provide conductivity to the material, even after printing. PEDOT: PSS has the highest efficiency among conductive organic materials, making it suitable for flexible and biodegradable electrical circuits.

Accurate modeling of the electrical conductivity of metallic and polymer microstructures is critical in predicting and optimizing the performance of these materials. These simulations, when combined with physical measurement, can provide a comprehensive understanding of the material's electrical characteristics, which is invaluable for various applications. PEDOT: PSS is an example of a conductive polymer mixture that can be used in flexible and biodegradable electrical circuits due to its high efficiency.

4.4.1 Simulation

To understand the performance of metallic deposition over microstructures for conductivity, various designs were simulated using COMSOL Multiphysics. These designs ranged from simple rectangular and semicircular forms to more intricate designs such as the ASU symbol over a conductive polymer layer. To compare the performance of these designs, a basic copper layer deposited over a cube was also simulated. A complex microstructure design over a polymer layer was also analyzed. Each simulation was performed once, using the COMSOL CAD designer to create distinct and unique designs which were then simulated for electric current. The simulation results were presented through a color-coded readout, where red areas depicted higher potential while blue areas showed lower potential. Contour lines were used to show how the potential varied with the geometry. By applying a voltage of 10V at one end of the copper coating and

grounding the other end, the simulation was able to determine how the microstructure affected the electric potential distribution. The unevenness formed by the metallic structures directly impacted the distribution of the electric potential.

By predicting the conductivity and resistivity of the material, the simulation provided valuable insight into how these microstructures would perform under different conditions. The simulation of metallic and polymer microstructures is crucial for optimizing their performance in a wide range of applications, including electronics, energy storage, and sensors. By accurately modeling the electrical conductivity of these materials, researchers can identify potential issues and make improvements to enhance their performance. Further, a digital multimeter was used to measure the resistance of 3D-printed parts.

The first test case (Figure 21a) involved simulating a uniform linear layer of copper over a conductive polymer. The top layer was made of copper, while the bottom layer consisted of a conductive polymer. A voltage of 10V was applied to the right part of the copper layer, while the left part was grounded. The colors used in the simulation represent the concentration of electric potential in the geometry, while the contour lines show the level at which the potential varies in the geometry. By varying the thickness of the copper layer from 0.1mm to 0.3mm, the simulation was able to show how the region of high electric potential changed concerning the thickness of copper on the conductive polymer. To assess the effects of microstructure on the variation of electric potential, three additional test cases were simulated. In each case, a copper layer was sandwiched between microstructures made up of conductive polymer. The microstructures used in these tests were a

rectangular structure with equal length and width (Figure 21b), a trapezoidal structure with a bottom length equal to the gap between consecutive trapezoidal structures (Figure 21c), and a semicircular structure with a radius equal to the gap between structures (Figure 21d). The thickness of the copper layer was varied from 0.1mm to 0.3mm to observe the variation of electric potential with thickness. One end of the copper layer was set to a 10V electric potential, while the other end was grounded. The red areas indicated high potential near the copper boundary, while blue areas represented ground on the other end of the sandwiched copper layer. The contour lines showed the exact level at which the potential varied across the geometry, illustrating major changes in the copper layer region. Each design showed different variations in terms of color contour and the direction followed by the contour lines.

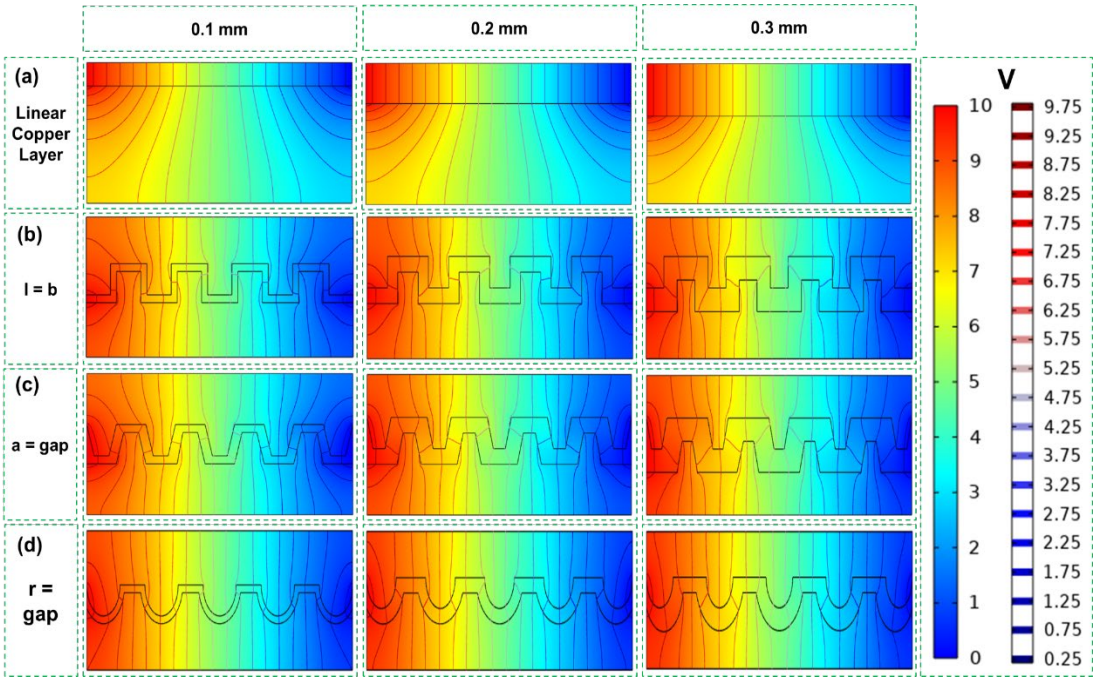

Figure 21: Electrical Conductivity COMSOL Simulation a) linear deposition b) rectangular microstructure c) trapezoidal microstructure d) semicircular microstructure.

Two more complex geometries were simulated to investigate the variation of electric potential within the design domain. In the first design, a complex microstructure made of copper was added on top of the rectangular conductive polymer part (Figure 22a). The microstructures were rectangular in shape with equal length and width, all facing inward. The microstructure on the left side was kept at 10V, while the one on the right side was grounded. For the second design, the letters ASU were made of copper on top of the rectangular conductive polymer part (Figure 22b). The bottom part of the letter A was kept at an electric potential of 10V, while the top part of the letter U was grounded. The contour lines illustrated the variation of electrical potential across the geometry using a color mapping scheme, where red represented areas of higher electric potential, and blue represented 0V of electric potential.

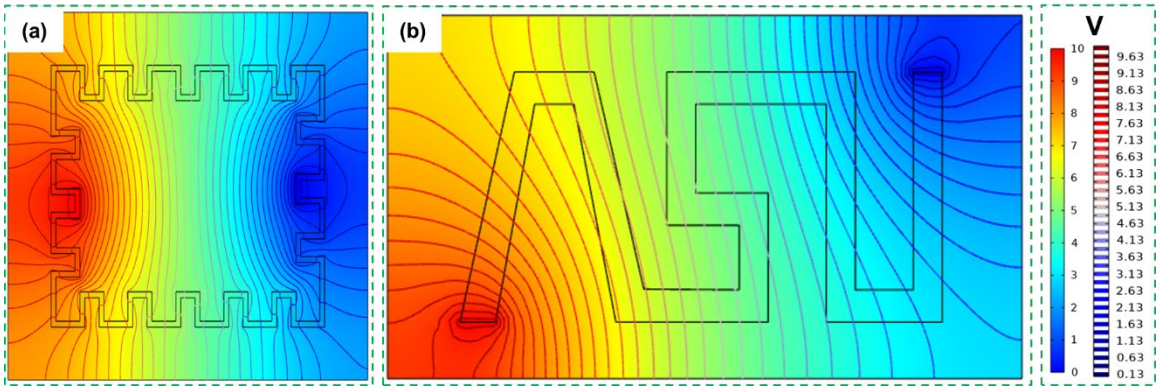

Figure 22: Electrical Conductivity COMSOL Simulation a) complex microstructure b) ASU.

4.4.2 Physical test

The electrical resistance of an object is a measure of its resistance to the flow of electrical current. Polyethylene glycol diacrylate (PEGDA) without any conductive fillers is an inductor, and to make it a conductor, a pellet based on PEDOT: PSS was added as a conductive organic material. To determine the

electrical resistance of various printed samples, a multimeter was used for physical measurement. For a thin film printed using a photocurable electrolyte solution, resistance was measured by placing two probes at separate ends of the thin film. The resistance was approximately 298k Ω when the film was dry, and it dropped to 135k Ω when it was wet. In the case of a 3D-printed cube, the resistance was around 128k Ω when it was dry, and it dropped down to 74.5k Ω when it was wet. After deposition, the cubes were tested for resistance between the gaps where all the copper was deposited. The cube with rectangular microstructure had a resistance of 25k Ω, whereas the cube with trapezoidal microstructure had a resistance of 18k Ω. The cube with circular microstructures had the lowest resistance of all, which was 12k Ω.

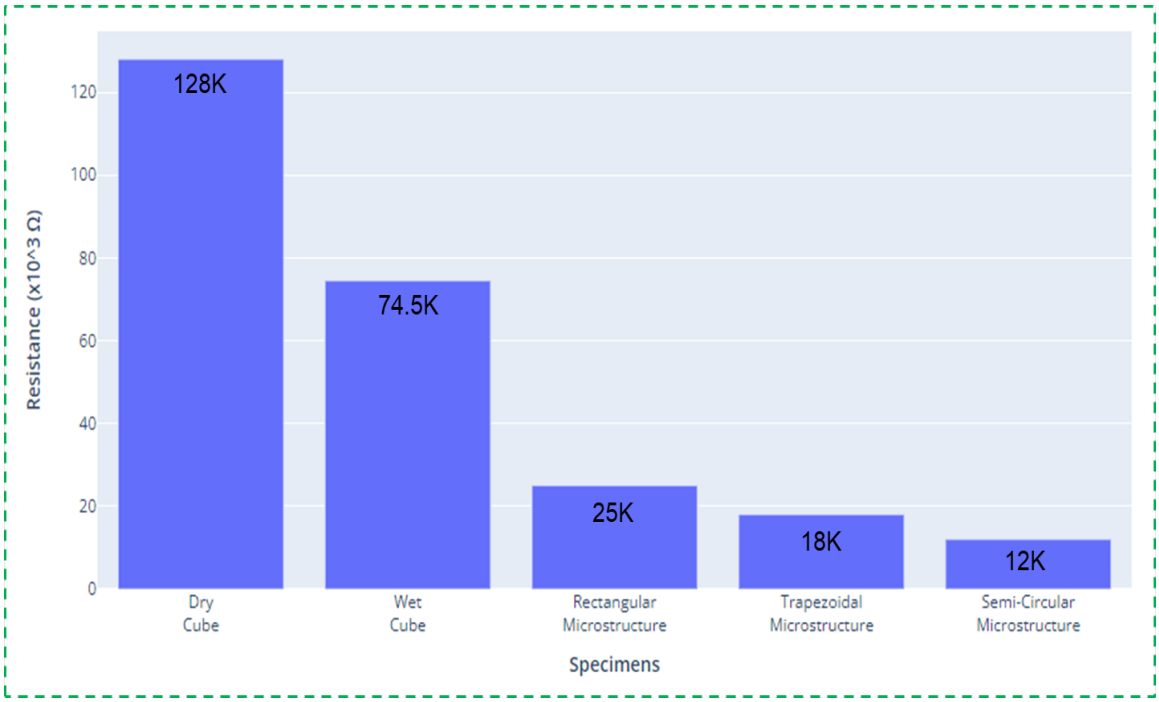

Figure 23: Bar graph for Resistance Vs Specimens

The circular microstructures had the best deposition results, which resulted in lower resistance compared to the other microstructures (Figure 23). However, due to the non-uniform deposition of copper and the very high resistance of the 3D-printed cubes, the overall resistance remained very high even after deposition.

4.5 Modelling of mechanical performance with metallic and polymer microstructures

Tensile testing is a destructive procedure employed to determine the tensile strength, yield strength, and ductility of a test specimen, usually made of plastic or composite materials. The test involves measuring the amount of force required to break the specimen and the degree to which it stretches or elongates before breaking. In complex loading scenarios, the von Mises stress is used to predict the yielding of materials, based on the results of uniaxial tensile tests. The von Mises stress satisfies the criterion that two stress states with equal distortion energy have an equal von Mises stress. The mechanical performance of metallic and polymer microstructures can be modeled using COMSOL Multiphysics software, which includes a CAD designer for creating models. A tensile test bar was created in compliance with ASTM standards to evaluate the bonding between a copper layer and polymer parts. The copper layer was placed between the polymer components, and the simulation aimed to measure the levels of von Mises stress on the interface under different design configurations. A total of 27 simulations were conducted, each featuring a unique microstructure design and a different thickness of copper layer sandwiched between the polymer components.

Simulations were performed using copper layers of 0.1mm, 0.2mm, and 0.3mm in thickness. The lower end of the specimen was fixed in place, while a perpendicular force of 10N was applied at the upper boundary.

The initial test involved using rectangular microstructures to sandwich a copper layer. Increasing the thickness of the copper layer led to a significant reduction in von Mises stress. Interestingly, the stress levels at the far ends of the copper layer were much lower than those in the middle section. The first simulation maintained an equal length and width of the rectangular microstructure (Figure 24a), which resulted in very high-stress levels. However, increasing the thickness of the copper layer led to a reduction in stress.

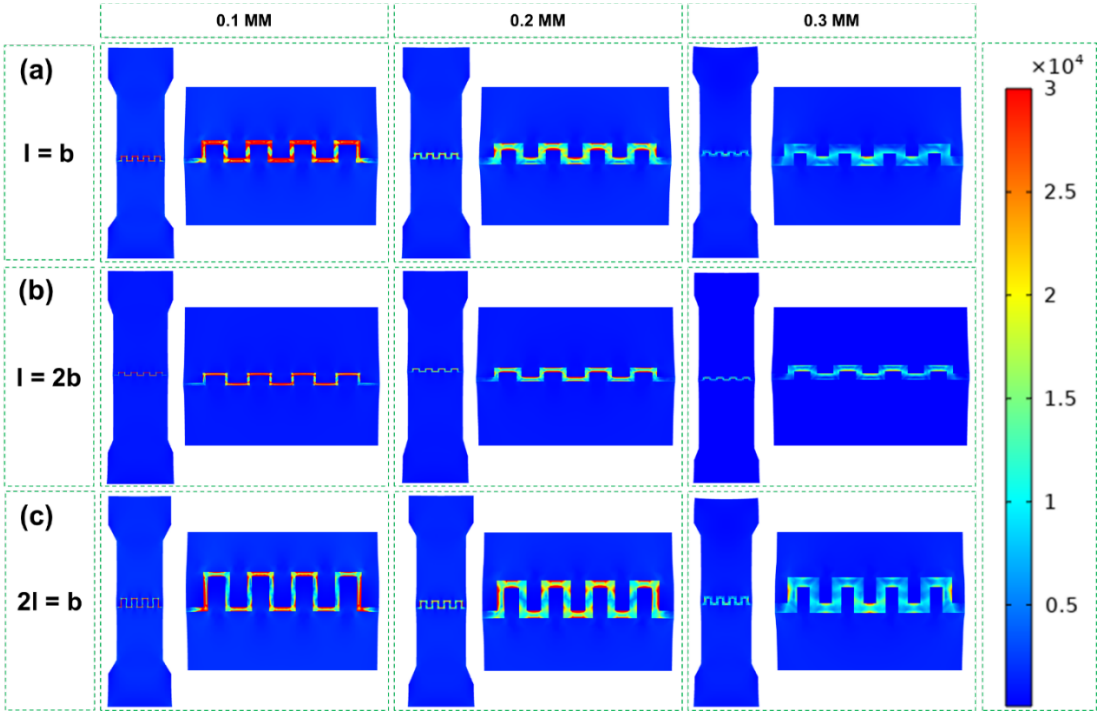

Figure 24: Tensile Test COMSOL Simulation a) length and width of the microstructure equal b) length of microstructure is twice of width c) width of the microstructure is twice the length.

In the second simulation, the width of the microstructure was twice the length (Figure 24b). Similar to the first simulation, increasing the thickness of the copper layer resulted in lower stress levels. The third simulation had a length twice the width of the microstructure (Figure 24c). This simulation produced the best result, with significantly lower stress levels than the other simulations, even with a copper layer thickness of only 0.1mm.

A copper layer was placed between trapezoidal microstructures in the second test. Von Mises stress was considerably reduced as the copper layer's thickness was increased. Contrary to the outcomes of the earlier simulations, the stress levels at the far ends of the copper layer were noticeably higher than those in the intermediate part. In the initial simulation, trapezoidal microstructures were used,

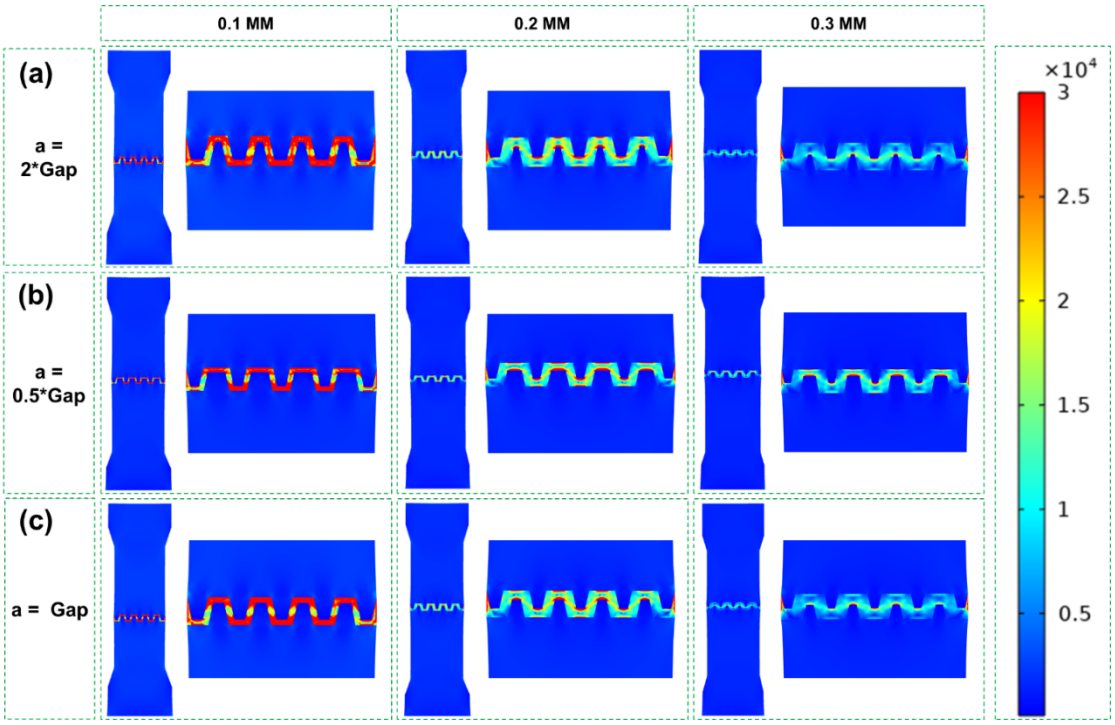

Figure 25: Tensile test COMSOL Simulation a) the bottom length of the trapezium is equal to the gap b) the bottom length of the trapezium is twice the gap c) the bottom length of the trapezium is half the gap.

with the bottom length being double the distance between each microstructure (Figure 25a). This caused the copper and polymer interaction to experience extremely high amounts of stress. Yet, the stress decreased as the copper layer's thickness increased. In the second simulation, the microstructure's bottom length was half that of the microstructures' distance from one another (Figure 25b). The copper layer's thickness was increased, like in the first simulation, and this resulted in reduced stress levels. The bottom length of the trapezoidal microstructure was equal to the space between microstructures in the third simulation (Figure 25c). Remarkably, no matter the size of the microstructures used in the simulations, the results were identical; the only difference was that the stress decreased as the copper layer's thickness increased.

The third test used semi-circular microstructures and sandwiched copper between polymer structures. The results of the simulation were equivalent to those of the earlier experiments. The copper layer's extreme ends saw significantly less stress than its center, in contrast to the trapezoidal models. In the original simulation, semicircle microstructures with a radius equal to half their distance apart were used (Figure 26a). High-stress levels were a result of the copper-polymer contact. Yet, the tension was reduced when the copper layer's thickness was increased. In the second simulation, the microstructure's radius was twice as long as the distance between them (Figure 26b). Like the first simulation, the stress levels fell when the copper layer's thickness was increased. The third simulation had a semi-circular microstructure with a radius equal to the distance between them (Figure 26c). Intriguingly, semi-circular microstructures in all simulations

yielded the same outcomes regardless of the dimensions of the microstructures, with the sole difference being a decrease in stress with increasing copper layer thickness.

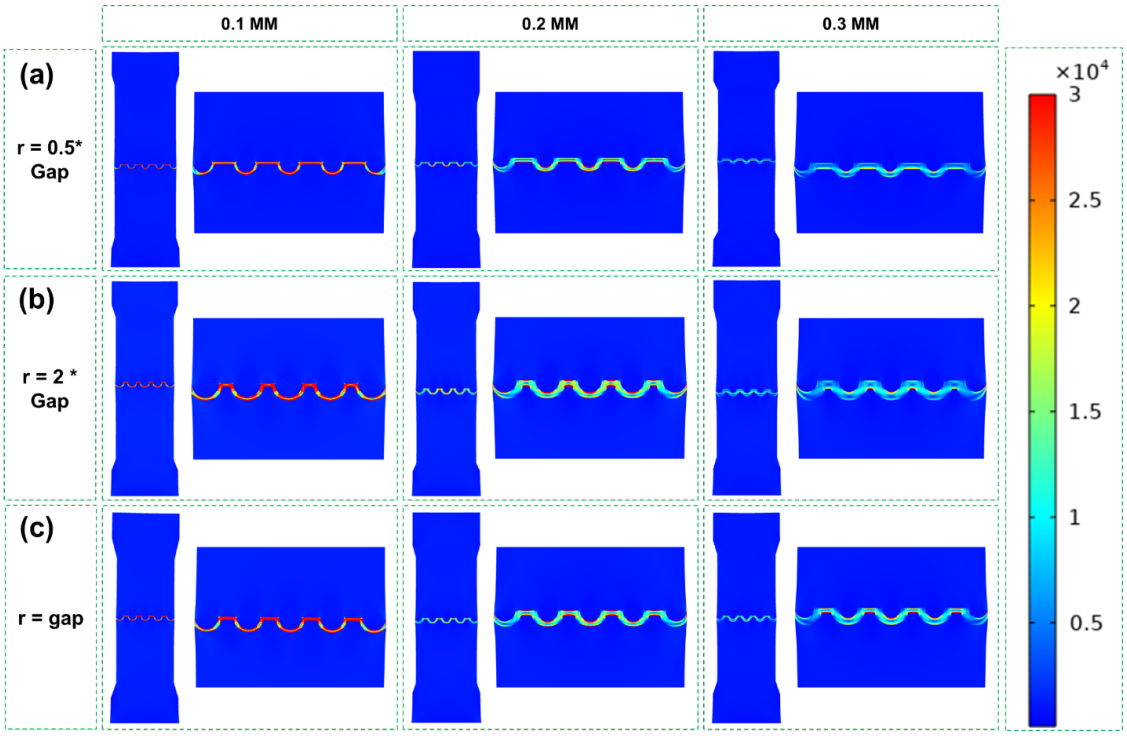

Figure 26: Tensile test COMSOL Simulation a) the radius of the semi-circle is half of the gap b) the radius of the semi-circle is twice the gap c) the radius of the semi-circle is equal to the gap.

CHAPTER 5 CONCLUSION AND FUTURE WORK

5.1 Conclusion

The study utilized an electrical field-assisted heterogeneous material printing (EFA-HMP) method to produce polymer materials with metallic microstructures using a composite of PEGDA and PEDOT: PSS polymer-based photocurable and conductive materials. The research successfully created a photocurable electrolyte composite and examined its curing properties, printability, and electrical field-assisted deposition performance on a thin film. The findings demonstrated the successful manufacture of microstructures with high precision and accuracy by presenting three distinct microstructures. Furthermore, the technique was expanded to incorporate metal deposition onto the printed structures using an electrical field-assisted process. The optimization of the process involved adjusting the voltage and deposition time. Physics-assisted simulations were used to explore the deposition process and optimize printing parameters.

Overall, this study introduced a novel additive manufacturing technique to investigate the impact of microstructure on deposition thickness. The research analyzed and experimentally validated the relationship between material properties, manufacturing process parameters, and surface structure and geometry parameters. The results were obtained by utilizing analytical models and experimental data to assess the impact of manufacturing parameters and material characteristics on the geometries of printed surface structures. The research opens exciting possibilities for producing polymer/metallic hierarchical structures using this technique.

5.2 Outlook

In recent years, the use of microstructures in materials engineering has gained significant attention for its ability to enhance mechanical performance. Metallic and polymer materials have been developed with desired properties through the creation of microstructures, providing a new avenue for materials engineers. Our research on the preparation of photocurable electrolyte composites and electrical field-assisted printing methods shows promise in improving manufacturing efficiency and reducing costs in the field of heterogeneous material manufacturing. This method allows for the printing of polymer/metallic hierarchical structures with broad application prospects. Our future work will focus on studying the bonding adhesion between metallic structures and polymers through tensile testing of various microstructures. Additionally, we aim to improve the conductivity of the photocurable electrolyte resin to achieve better copper deposition results and execute the deposition of other metals too. We plan to study the enhancement of bio-inspired heterogeneous material structures using the proposed printing method.

REFERENCES

[1]. Wang, X., Jiang, M., Zhou, Z., Gou, J., & Hui, D. (2017). 3D printing of polymer matrix composites: A review and prospective. Composites Part B: Engineering, 110, 442-458.

[2]. Yang, Y., Song, X., Li, X., Chen, Z., Zhou, C., Zhou, Q., & Chen, Y. (2018). Recent progress in biomimetic additive manufacturing technology: from materials to functional structures. Advanced Materials, 30(36), 1706539.

[3]. Yao, H., Dao, M., Imholt, T., Huang, J., Wheeler, K., Bonilla, A., ... & Ortiz, C. (2010). Protection mechanisms of the iron-plated armor of a deep-sea hydrothermal vent gastropod. Proceedings of the National Academy of Sciences, 107(3), 987-992.

[4]. Seol, S. K., Kim, D., Lee, S., Kim, J. H., Chang, W. S., & Kim, J. T. (2015). Electrodeposition-based 3D printing of metallic microarchitectures with controlled internal structures. Small, 11(32), 3896-3902.

[5]. Delmonte, J. (2013). Metal/polymer composites. Springer.

[6]. Hudkins, J. R., Wheeler, D. G., Peña, B., & Berlinguette, C. P. (2016). Rapid prototyping of electrolyzer flow field plates. Energy & Environmental Science, 9(11), 3417-3423.

[7]. Rosa-Ortiz, S. M., Kadari, K. K., & Takshi, A. (2018). Low-temperature soldering surface-mount electronic components with hydrogen-assisted copper electroplating. MRS Advances, 3, 963-968.

[8]. Lazarus, N., Bedair, S. S., Hawasli, S. H., Kim, M. J., Wiley, B. J., & Smith, G. L. (2019). Selective Electroplating for 3D-Printed Electronics. Advanced Materials Technologies, 4(8), 1900126.

[9]. Angel, K., Tsang, H. H., Bedair, S. S., Smith, G. L., & Lazarus, N. (2018). Selective electroplating of 3D printed parts. Additive Manufacturing, 20, 164-172.

[10]. Hensleigh, R., Cui, H., Xu, Z., Massman, J., Yao, D., Berrigan, J., & Zheng, X. (2020). Charge-programmed three-dimensional printing for multi-material electronic devices. Nature Electronics, 3(4), 216-224.

[11]. Zhao, Z., Bai, J., Yao, Y., & Wang, C. (2020). Printing continuous metal structures via polymer-assisted photochemical deposition. Materials Today, 37, 10-17.

[12]. Yang, X., Sun, M., Bian, Y., & He, X. (2019). A Room-Temperature High-Conductivity Metal Printing Paradigm with Visible-Light Projection Lithography. Advanced Functional Materials, 29(1), 1807615.

[13]. Warr, C., Valdez, J. C., Bickham, B. P., Knight, C. J., Franks, N. A., Chartrand, N., ... & Cook, A. D. (2020). Biocompatible PEGDA resin for 3D printing. ACS applied biomaterials, 3(4), 2239-2244.

[14]. Li, X., Yang, Y., Xie, B., Chu, M., Sun, H., Hao, S., ... & Chen, Y. (2019). 3D printing of flexible liquid sensor based on swelling behavior of hydrogel with carbon nanotubes. Advanced Materials Technologies, 4(2), 1800476.

[15]. Tang, T., Ahire, B., & Li, X. (2023). Scalable multi-material additive manufacturing of bioinspired polymeric material with metallic structures via electrically assisted stereolithography. Journal of Manufacturing Science and Engineering, 145(1), 011004.

[16]. Suchentrunk, R. (2004). Metal matrix composites are produced by electroplating. a review of technology and applications. Nanostructured Thin Films and Nanodispersion Strengthened Coatings, 241-250.

[17]. Ambrosi, A., & Pumera, M. (2016). 3D-printing technologies for electrochemical applications. Chemical Society reviews, 45(10), 2740-2755.

[18]. Hemsley, S. J., & Zhou, W. (2010). Platinum plating for turbine blades: technology development and process improvement. Transactions of the IMF, 88(1), 11-16.

[19]. Hawatmeh, D., Rojas-Nastrucci, E., & Weller, T. (2016, February). A multi-material 3D printing approach for conformal microwave antennas. In 2016 International Workshop on Antenna Technology (iWAT) (pp. 7-10). IEEE.

[20]. Bahr, R. A., Fang, Y., Su, W., Tehrani, B., Palazzi, V., & Tentzeris, M. M. (2017, June). Novel uniquely 3D printed intricate Voronoi and fractal 3D antennas. In 2017 IEEE MTT-S International Microwave Symposium (IMS) (pp. 1583-1586). IEEE.

[21]. Bernasconi, R., Carrara, E., Hoop, M., Mushtaq, F., Chen, X., Nelson, B. J., ... & Magagnin, L. (2019). Magnetically navigable 3D printed multifunctional microdevices for environmental applications. Additive Manufacturing, 28, 127-135.

[22]. Xie, Y., Ye, S., Reyes, C., Sithikong, P., Popa, B. I., Wiley, B. J., & Cummer, S. A. (2017). Microwave metamaterials made by fused deposition 3D printing of a highly conductive copper-based filament. Applied Physics Letters, 110(18), 181903.

[23]. Murzin, S. P., Palkowski, H., Melnikov, A. A., & Blokhin, M. V. (2022). Laser welding of metal-polymer-metal sandwich panels. Metals, 12(2), 256.

[24]. Patel, A. R., Dalwadi, C. G., & Rana, H. G. (2016). A review: dissimilar material joining of metal to polymer using friction stir welding (FSW). Int J Sci Technol Eng, 2(10), 702-706.

[25]. Trzepieciński, T., Najm, S. M., Sbayti, M., Belhadjsalah, H., Szpunar, M., & Lemu, H. G. (2021). New advances and future possibilities in forming technology of hybrid metal–polymer composites used in aerospace applications. Journal of Composites Science, 5(8), 217.

[26]. Tosto, C., Tirillò, J., Sarasini, F., & Cicala, G. (2021). Hybrid metal/polymer filaments for fused filament fabrication (FFF) to print metal parts. Applied Sciences, 11(4), 1444.

[27]. Nabipour, M., Akhoundi, B., & Bagheri Saed, A. (2020). Manufacturing of polymer/metal composites by fused deposition modeling process with polyethylene. Journal of Applied Polymer Science, 137(21), 48717.

[28]. Kwang, K., & Shahinpoor, M. (2003). Ionic polymer–metal composites: II. Manufacturing. Smart Mater Struct, 12, 65-79.

[29]. Guymon, G. G., & Malakooti, M. H. (2022). Multifunctional liquid metal polymer composites. Journal of Polymer Science, 60(8), 1300-1327.

[30]. Gazotti, W. A., Nogueira, A. F., Girotto, E. M., Micaroni, L., Martini, M., das Neves, S., & De Paoli, M. A. (2001). Optical devices based on conductive polymers. In Handbook of advanced electronic and photonic materials and devices (pp. 53-98). Academic Press.

[31]. Lubimyi, N. S., Polshin, A. A., Gerasimov, M. D., Tikhonov, A. A., Antsiferov, S. I., Chetverikov, B. S., ... & Ridvanov, İ. (2022). Justification of the use of composite metal-metal-polymer parts for functional structures. Polymers, 14(2), 352.

[32]. Masood, S. H., & Song, W. Q. (2004). Development of new metal/polymer materials for rapid tooling using fused deposition modeling. Materials & Design, 25(7), 587-594.

[33]. Chung, C. K., Hong, Y. Z., & Chang, W. T. (2007). Fabrication of the monolithic polymer–metal microstructure by the backside exposure and electroforming technology. Microsystem Technologies, 13, 531-536.

[34]. Huang, J., Qin, Q., & Wang, J. (2020). A review of stereolithography: Processes and systems. Processes, 8(9), 1138.

[35]. Jacobs, P. F. (1992). Fundamentals of stereolithography. In 1992 international solid freeform fabrication symposium.

[36]. Zissi, S., Bertsch, A., Jézéquel, J. Y., Corbel, S., Lougnot, D. J., & Andre, J. C. (1996). Stereolithography and microtechniques. Microsystem technologies, 2, 97-102.

[37]. Pham, D. T., & Ji, C. (2000). Design for stereolithography. Proceedings of the Institution of Mechanical Engineers, Part C: Journal of Mechanical Engineering Science, 214(5), 635-640.

[38]. Choi, J. W., Kim, H. C., & Wicker, R. (2011). Multi-material stereolithography. Journal of Materials Processing Technology, 211(3), 318-328.

[39]. Abbott, A. P., Frisch, G., & Ryder, K. S. (2013). Electroplating using ionic liquids. Annual Review of Materials Research, 43, 335-358.

[40]. Boulanger, C. (2010). Thermoelectric material electroplating: a historical review. Journal of Electronic Materials, 39, 1818-1827.

[41]. Augustyn, P., Rytlewski, P., Moraczewski, K., & Mazurkiewicz, A. (2021). A review on the direct electroplating of polymeric materials. Journal of Materials Science, 56(27), 14881-14899.

[42]. Calvert, P., Duggal, D., Patra, P., Agrawal, A., & Sawhney, A. (2008). Conducting polymer and conducting composite strain sensors on textiles. Molecular Crystals and Liquid Crystals, 484(1), 291-657.

[43]. De Leeuw, D. M., Kraakman, P. A., Bongaerts, P. F. G., Mutsaers, C. M. J., & Klaassen, D. B. M. (1994). Electroplating of conductive polymers for the metallization of insulators. Synthetic metals, 66(3), 263-273.

[44]. Joyee, E. B., Lu, L., & Pan, Y. (2019). Analysis of mechanical behavior of 3D printed heterogeneous particle-polymer composites. Composites Part B: Engineering, 173, 106840.